Mitochondrial CLPP2 Assists Coordination and Homeostasis of Respiratory Complexes[1][OPEN]

Jakob Petereit,[a] Owen Duncan,[a] Monika W. Murcha,[a] Ricarda Fenske,[a] Emilia Cincu,[a] Jonathan Cahn,[a] Adriana Pružinská,[a] Aneta Ivanova,[a] Laxmikanth Kollipara,[b] Stefanie Wortelkamp,[b] Albert Sickmann,[b,c,d] Jiwon Lee,[e] Ryan Lister,[a,f] A. Harvey Millar,[a,2,3] and Shaobai Huang[a,3]

[a]ARC Centre of Excellence in Plant Energy Biology, School of Molecular Sciences, The University of Western Australia, Washington 6009, Australia
[b]Leibniz-Institut für Analytische Wissenschaften-ISAS-e.V., 44139 Dortmund, Germany
[c]Department of Chemistry, College of Physical Sciences, University of Aberdeen, Aberdeen AB24 3FX, Scotland, United Kingdom
[d]Medizinische Fakultät, Medizinische Proteom-Center, Ruhr-Universität Bochum, D–44801 Bochum, Germany
[e]Centre for advanced Microscopy, The Australian National University, Acton, Australian Capital Territory 2601, Australia
[f]The Harry Perkins Institute of Medical Research, Perth, Washington 6009, Australia

ORCID IDs: 0000-0003-2159-0380 (J.P.); 0000-0002-3689-6158 (M.W.M.); 0000-0002-0906-8525 (R.F.); 0000-0002-5006-741X (J.C.); 0000-0002-2465-7213 (A.I.); 0000-0002-2673-0488 (L.K.); 0000-0003-2382-2106 (J.L.); 0000-0001-6637-7239 (R.L.); 0000-0001-9679-1473 (A.H.M.); 0000-0003-3667-611X (S.H.).

Protein homeostasis in eukaryotic organelles and their progenitor prokaryotes is regulated by a series of proteases including the caseinolytic protease (CLPP). CLPP has essential roles in chloroplast biogenesis and maintenance, but the significance of the plant mitochondrial CLPP remains unknown and factors that aid coordination of nuclear- and mitochondrial-encoded subunits for complex assembly in mitochondria await discovery. We generated knockout lines of the single gene for the mitochondrial CLP protease subunit, *CLPP2,* in Arabidopsis (*Arabidopsis thaliana*). Mutants showed a higher abundance of transcripts from mitochondrial genes encoding oxidative phosphorylation protein complexes, whereas nuclear genes encoding other subunits of the same complexes showed no change in transcript abundance. By contrast, the protein abundance of specific nuclear-encoded subunits in oxidative phosphorylation complexes I and V increased in CLPP2 knockouts, without accumulation of mitochondrial-encoded counterparts in the same complex. Complexes with subunits mainly or entirely encoded in the nucleus were unaffected. Analysis of protein import and function of complex I revealed that while function was retained, protein homeostasis was disrupted, leading to accumulation of soluble subcomplexes of nuclear-encoded subunits. Therefore, CLPP2 contributes to the mitochondrial protein degradation network through supporting coordination and homeostasis of protein complexes encoded across mitochondrial and nuclear genomes.

Mitochondria contain numerous protein complexes that catalyze important functions, including oxidative phosphorylation leading to ATP synthesis, respiratory carbon metabolism, consumption of oxygen, and the production of reactive oxygen species (ROS; Millar et al., 2011; Huang et al., 2016). Subunits for some of these protein complexes are encoded across mitochondrial and nuclear genomes. This requires separate gene expression, protein synthesis, and protein import into mitochondria followed by a coordinated complex assembly. The regulation at a transcriptional level is limited, owing to the general lack of specific mitochondrial gene transcript activation (Costanzo and Fox, 1990; Giegé et al., 2000; Kühn et al., 2009).

Some of the coordination of nuclear- and mitochondrial-encoded protein complex assembly in yeast occurs at the translation level and is unidirectional (Couvillion et al., 2016), with cytosolic events influencing mitochondrial mRNA levels. In Arabidopsis (*Arabidopsis thaliana*) cell culture under carbon starvation and refeeding conditions, a transient dysregulation in the stoichiometry of complex V subunits ATP1 and ATP2, encoded by mitochondrial and nuclear genomes, respectively, has been identified (Giegé et al., 2005). *ATP1* was increased at the transcript level but not at the level of ATP1 protein abundance, while ATP2 increased at the protein level, but the *ATP2* transcript was unchanged. Giegé et al. (2005) proposed that posttranslational processes in assembly were responsible for rebalancing this process after refeeding of cells, but they did not identify factors responsible for it. It has previously been suggested that unassembled protein complex subunit degradation by mitochondrial proteolysis is the basis for such regulation (Sarria et al., 1998), but the specific protease(s) involved have not been identified.

Organellar protease networks exist in mitochondria and plastids to control intraorganellar protein degradation (van Wijk, 2015). ATP-dependent endopeptidases of the AAA+ superfamily of ATPases associated

with various cellular activities, such as long-filament phenotype-1 (LON1), caseinolytic protease (CLPP), and filamentous temperature-sensitive H (FTSH), are the dominant components of these networks that are conserved across eukaryotes. In plants, mitochondrial LON1 acts as a chaperone, by stabilizing newly synthesized/imported proteins to aid proper folding, and as a protease, by degrading mitochondrial protein aggregates (Li et al., 2017). Loss of mitochondrial FTSHs leads to oxidative stress, and FTSHs are shown to be components of the defense against accumulation of carbonylated proteins in plant mitochondria (Smakowska et al., 2016). To date, there have not been any reports of the effect of loss of CLPP on plant mitochondria.

The CLPP protease has an active Ser-His-Asp catalytic triad and is widely present in bacteria, fungi, mammals, and plants (Yu and Houry, 2007; Bhandari et al., 2018). The x-ray structure of CLPP has been solved from several different organisms with similar features: the protease subunit is comprised of two heptameric rings forming a cylinder-like structure that encloses a large chamber containing the protease active sites (Yu and Houry, 2007; Bhandari et al., 2018). Some bacteria, such as the cyanobacterium *Synechococcus elongatus*, contain CLPR, which is an inactive version of CLPP lacking the catalytic triad (Schelin et al., 2002). In bacteria, CLPP forms complexes with the AAA+ chaperones CLPX and CLPA and acts as a selective filter for specific target substrates (Gerth et al., 2008).

Plants have a diversified and complex CLP family, with six active CLPPs (CLPP1–CLPP6) and four inactive CLPR paralogs (CLPR1–CLPR4) found in Arabidopsis (Sjögren et al., 2006; van Wijk, 2015). In addition, Arabidopsis have CLP/HSP100 AAA+ chaperones with seven class I CLPs (CLPB1–CLPB4, CLPC1 and CLPC2, and CLPD) in chloroplasts and three class II CLPs (CLPX1–CLPX3) in mitochondria (Peltier et al., 2004). Arabidopsis plastids have five CLPP proteases (CLPP1, encoded by the plastid genome, and CLPP3–CLPP6) and four inactive CLPRs, which together form the tetradecameric and asymmetric ~350-kD CLP protease core (van Wijk, 2015). Three CLP AAA+ chaperones (CLPC1, CLPC2, and CLPD) and the adaptor CLPS1 deliver protein substrates to the protease complex for degradation (van Wijk, 2015). Plastid *clpp* and *clpr* mutants in Arabidopsis display severe phenotypes, including disorder of embryogenesis, seedling development, and chloroplast biogenesis. Complete loss of CLPP5 and CLPP4 is embryo lethal, and the *clpp3* null mutant can only germinate and develop seedlings under heterotrophic conditions (Kim et al., 2013). CLPP1 is known to be essential for leaf development in tobacco (*Nicotiana tabacum*; Shikanai et al., 2001). Knockdown of a number of subunits of the CLP complex in tobacco impacted the CLP complex composition and chloroplastic protein homeostasis (Moreno et al., 2017, 2018). Knockout lines of CLPR2 or CLPR4 cause embryogenesis delay and developmental arrest at the cotyledon stage (Kim et al., 2009). Upregulation of chaperone proteins and downregulation of photosynthesis coupled with upregulation of the ATP import pathway occur in *clpr2*, *clpr4*, and *clpr3* mutants (Kim et al., 2013). Dysfunction of CLPP6 in rice causes developmental stage-dependent virescent yellow leaf with decreased chlorophyll accumulation and impaired photosynthesis (Dong et al., 2013). The proteolytic P-ring (CLPP) and the structurally similar R-ring (CLPR) form the core CLPPR complex. Therefore, the plant CLPPR protease complex appears to play an essential role in plastid and chloroplast biogenesis and development.

Arabidopsis mitochondria contain a homotetradecameric CLPP2 core protease encoded by a single nuclear gene and three CLPX chaperones (CLPX1–CLPX3; Peltier et al., 2004). The CLPP2 core has been detected by Blue Native PAGE (BN-PAGE) with a molecular mass of ~320 kD, consistent with a predicted tetradecamer structure (Peltier et al., 2004; Senkler et al., 2017), but no transfer DNA (T-DNA) lines for CLPP2 exist. In this study, we developed two knockout lines of *CLPP2* in Arabidopsis by mutations using CRISPR-Cas9 technology, providing a tool for functional analysis of mitochondrial CLPP2. Our assessments using a range of omic technologies and specific follow-up experiments have revealed that whereas CLPP2 is not essential for plant growth, it does contribute to the regulation of nuclear and mitochondrial

[1]This work was supported by the University of Western Australia (International Scholarship to J.P.); the Australian Research Council (discovery grant no. DP140101580 to S.H., A.P., and E.C.; grant nos. CE140100008 to A.H.M. and CE140100008 to R.L. and J.C.; Future Fellowship nos. FT130101338 to S.H. and FT130100112 to M.W.M.; and Discovery Early Career Research Award no. DE120102913 to A.P.); the Sylvia and Charles Viertel Senior Medical Research Fellowship (to R.L.); the Howard Hughes Medical Institute (International Research Scholarship to R.L.); the Ministerium für Kultur und Wissenschaft des Landes Nordrhein-Westfalen, the Der Regierende Bürgermeister von Berlin, Senatskanzlei Wissenschaft und Forschung (inkl. Wissenschaft und Forschung), the Bundesministerium für Bildung und Forschung (to L.K., S.W., and A.S.); and the National Collaborative Research Infrastructure Strategy (to J.L.).

[2]Author for contact: harvey.millar@uwa.edu.au.

[3]Senior authors.

The author responsible for distribution of materials integral to the findings presented in this article in accordance with the policy described in the Instructions for Authors (www.plantphysiol.org) is: Shaobai Huang (shaobai.huang@uwa.edu.au).

J.P. performed most of the experiments and data analysis; O.D. and R.F. assisted with and performed some of the mass spectrometry and data analysis; J.C., E.C., and R.L. assisted in the development of CRISPR-Cas9 knockout lines; A.P. assisted in RNA-sequencing analysis; L.K., S.W., and A.S. assisted with the ChaFRADIC, liquid chromatography-mass spectrometry, and data analysis; M.M. and A.I. assisted with in vitro imports; J.L. performed the transmission electron microscopy analysis; S.H., A.H.M., and J.P. designed experiments and analyzed and discussed results; S.H., A.H.M., and J.P. wrote the article; and all authors commented on the results and the article.

[OPEN]Articles can be viewed without a subscription.

www.plantphysiol.org/cgi/doi/10.1104/pp.20.00136

protein complex assembly and maintenance. The manner of CLPP2 function is consistent with previously proposed posttranslational processes that have been implicated in this control.

RESULTS

CRISPR-Cas9 Guided *CLPP2* Knockout Results in Two Stable Knockout Mutants

The Ser-type, ATP-dependent CLP protease system in Arabidopsis mitochondria contains a CLPP2 core subunit (AT5G23140) and three homologous CLPX chaperone subunits (CLPX1 [AT5Gg53350], CLPX2 [AT5G49840], and CLPX3 [AT1G33360]; van Wijk, 2015). So far, there is no reported or available T-DNA insertion line within the coding region for *CLPP2* (AT5G23140). To acquire independent stable *CLPP2* mutants, we used a CRISPR-Cas9 guided system to knock out the CLPP2 core subunit (Supplemental Fig. S1), resulting in two individual CRISPR-Cas9 mutants, *clpp2-1* and *clpp2-2*, showing a complete knockout of the target gene. Both mutations occurred within exon 1, as shown by guides, primers, and restriction sites/enzymes (Fig. 1A).

The first mutant, *clpp2-1*, showed two separate genetic events that caused the CLPP2 knockout: first, a single adenine insertion at the 25-bp position introduced a frame shift and disrupted the restriction site of NlaIV at 24 bp (Fig. 1B); and second, introduction of the adenine at CRISPR site 1 created a 3′ end identical to the 5′ end at CRISPR site 3. It is likely that this caused a second error from the nonhomologous end-joining (NHEJ) DNA repair mechanism or the alternative NHEJ DNA repair mechanism, microhomology-mediated end joining, known for insertions, deletions, and inversions (McVey and Lee, 2008), by inserting the complete fragment between CRISPR site 1 and CRISPR site 3 in a reverse-complemented orientation. Consequentially, five downstream stop codons (TGA or TAA) were generated and the second NlaIV restriction site was shifted to the position at 95 bp (Fig. 1B). The second mutant, *clpp2-2*, had a single NHEJ error at CRISPR site 2 with an adenine insertion at the position of 124 bp, resulting in a disruption of the NruI restriction site and the introduction of three downstream stop codons (TAA or TGA; Fig. 1B).

We confirmed the disruption of *CLPP2* in the mutants in the genetic sequence, as well as its consequence on mRNA and protein levels. As the two mutations resulted in disruption of restriction sites within exon 1, genomic DNA from mutants and the wild type was amplified using primers F1 and R1 (Fig. 1A) and digested with NlaIV for *clpp2-1* and NruI for *clpp2-2*. The NlaIV-digested wild-type PCR product resulted in three fragments, a long, 165-bp fragment between the first and second NlaIV restriction sites, an intermediate, 105-bp fragment from restriction site 2 to the 3′ end of the PCR product, and a short 24-bp fragment (out of gel range) from the 5′ end to restriction site 1 (Fig. 1C). For *clpp2-1*, NIaIV restriction site 1 was disrupted and restriction site 2 moved in a 5′-end direction. Accordingly, the restriction digest pattern had two fragments in total, a 199-bp fragment from the new restriction site 2 to the 3′ end of the PCR product and a 92-bp fragment from the 5′ end to the new restriction site 2 (Fig. 1C). The NruI-digested wild-type exon 1 PCR product resulted in two fragments 171 and 120 bp in length, whereas *clpp2-2* had a disrupted NruI restriction site and only showed the full 291-bp PCR product (Fig. 1C).

Based on RNA-sequencing (RNAseq) analysis, the transcript levels of *CLPP2* were significantly reduced in *clpp2-1* and *clpp2-2* to ~15% of the wild-type level (Fig. 1D). The expression levels of representative housekeeping genes such as general *TUBULIN6* (AT5G12250) and mitochondrial *ATVDAC1* (AT3G01280) were unaffected in both mutants (Fig. 1D). Whereas CRISPR-Cas9 systems should not actively alter transcript levels, the introduced frameshifts forming several stop codons in the sequence of *CLPP2*, >50 bp away from the exon-exon junction (Fig. 1B), created a high-confidence position for exon-exon junction nonsense-mediated mRNA decay, which may contribute to the observed low transcript abundance (Lloyd, 2018).

To detect the protein abundance of CLPP2, we isolated mitochondria and conducted multiple reaction monitoring (MRM)-based targeted proteomic analysis and included the theoretical peptide of the inverted CLPP2-1 section. The peptide MRM transitions are presented in Supplemental Table S1. CLPP2 protein abundance in mitochondria from both mutants was undetectable, whereas all selected peptides of CLPP2 were detected in the wild type (Fig. 1E). We also did not detect any evidence of theoretical CLPP2-1 peptides. Two representative mitochondrial housekeeping proteins (mitochondrial heat shock protein 70 [mtHSP70; AT4G37910] and a voltage-dependent ion channel [ATVDAC2–AT5G67500]) showed no significant change in protein abundance in either mutant (Fig. 1E). The virtual absence of CLPP2 proteins in both mutants could be explained by the introduction of stop codons at the first exon (Fig. 1B) that fully disrupted the translation of any functional CLPP2 protein.

Loss of CLPP2 Has an Impact on Transcript Levels of Mitochondrial Genes But Little Effect on Expression of Nuclear Genes

To evaluate global transcript abundance changes upon the loss of mitochondrial CLPP2, we used high-throughput RNAseq to find and quantify differentially expressed genes (DEGs). We analyzed the transcriptome of hydroponically grown seedlings of *clpp2-1*, *clpp2-2*, and the wild type, with three biological replicates for each genotype. Based on a filter of a log2 fold change (log2FC) exceeding ± 0.4 and adjusted *P*-values of ≤ 0.05, we identify 62 DEGs using the R package Deseq2 (Love et al., 2014), which showed a consistent

pattern in both mutants (Fig. 2). Only 0.1% of nuclear gene transcripts had significant changes in abundance in *clpp2-1* and *clpp2-2*. This was considerably lower than the 33% of mitochondrial transcripts that showed significant changes in abundance in both mutants (Fig. 2), indicating that disruption of *CLPP2* has a specific impact on the abundance of transcripts from mitochondrial genes.

In *clpp2-1* and *clpp2-2*, 41 of the 54 upregulated DEGs from nuclear and mitochondrial genomes encode mitochondrial-localized proteins, whereas three of eight downregulated DEGs other than *CLPP2* encode a mitochondrial-localized protein (Table 1). Two genes that encode nonmitochondrial targeted proteins and have unknown function stand out, showing very high and consistent log2FC values. AT4G36850 encodes a conserved PQ-Motif protein (Pfam [PF04193], involved in lysosome targeting) and AT3G56730 encodes a putative endonuclease with a conserved LabA-like PIN domain of limkain b1 (cd10910), which is a common

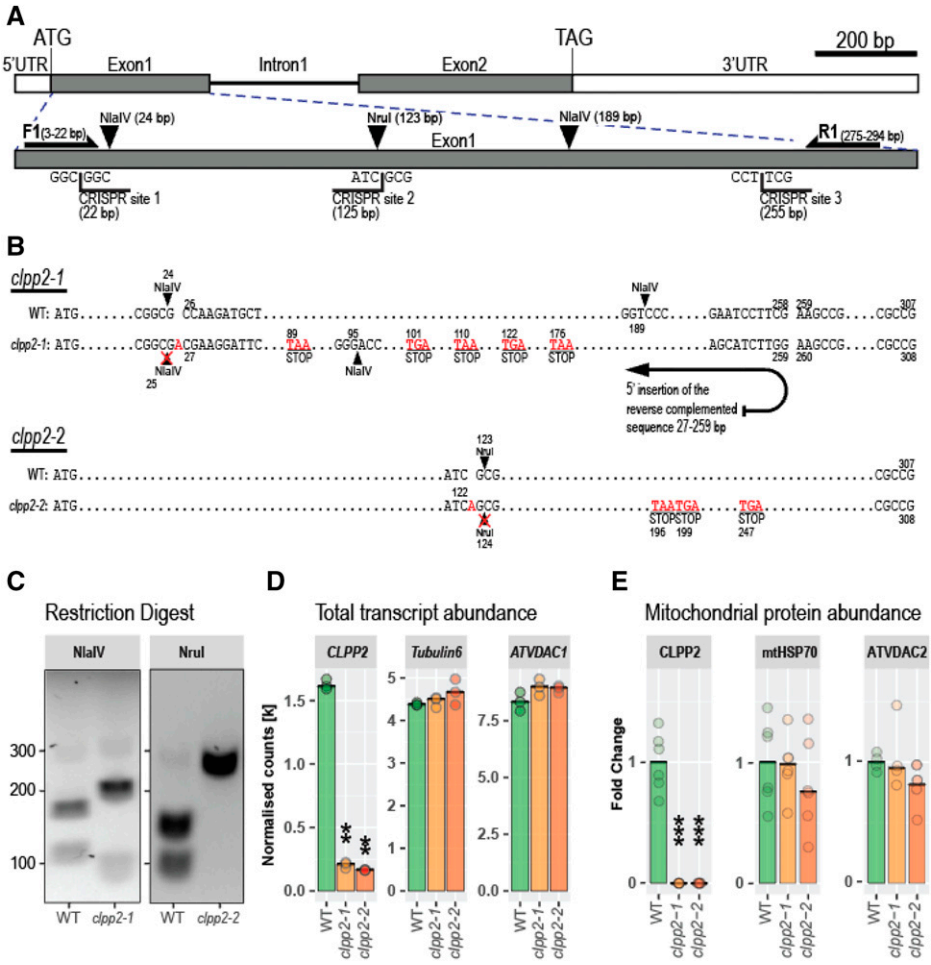

Figure 1. Development of two independent *CLPP2* mutants using CRISPR-Cas9. A, Layout of the CLPP2 gene structure, with enlargement of exon 1 showing CRISPR-Cas9 target sites, primer positions, and restriction sites used for restriction digest-based confirmation of the mutations. UTR, Untranslated region. B, Mapping of CRISPR-Cas9 gene disruption for wild-type (WT) CLPP2 and two individual knockouts, *clpp2-1* and *clpp2-2*. For the *Clpp2-1* map, the wild type shows the exon 1 sequence map with the location of two NlaIV restriction sites. *Clpp2-1* has an adenine insertion (A) at CRISPR site 1 disrupting (X) one NlaIV restriction site and an insertion of the reverse complemented wild-type sequence between CRISPR site 1 and CRISPR site 3, introducing five stop codons (TAA, TGA) resulting in a change of the second NlaIV restriction site. For the *Clpp2-2* map, the wild type shows the exon 1 sequence map with the location of one NruI restriction site. *Clpp2-2* has an A insertion (CRISPR site 2) resulting in the disruption of the NruI restriction site and insertion of three stop codons. C, Confirmation of CRISPR-Cas9 gene disruption based on PCR fragment restriction digest amplified by forward (F1) and reverse (R1) primers. D, Confirmation of CRISPR-Cas9 gene disruption at the transcript level based on RNAseq analysis. Normalized counts of the target gene, *CLPP2*, and the two control genes, *Tubulin6* and *ATVDAC1*, are presented. Asterisks indicate significant difference (**$P \leq 0.01$; $n = 3$). E, Confirmation of CRISPR-Cas9 gene disruption at the protein level based on a targeted proteomic approach. Fold changes of the target protein CLPP2 and the two control proteins, mtHSP70 and ATVDAC2, are presented. Asterisks indicate significant difference (***$P \leq 0.0001$; $n = 3$ peptides with two replicates for CLPP2, 3 peptides with two replicates for mtHSP70, and 2 peptides with two replicates for ATVDAC2).

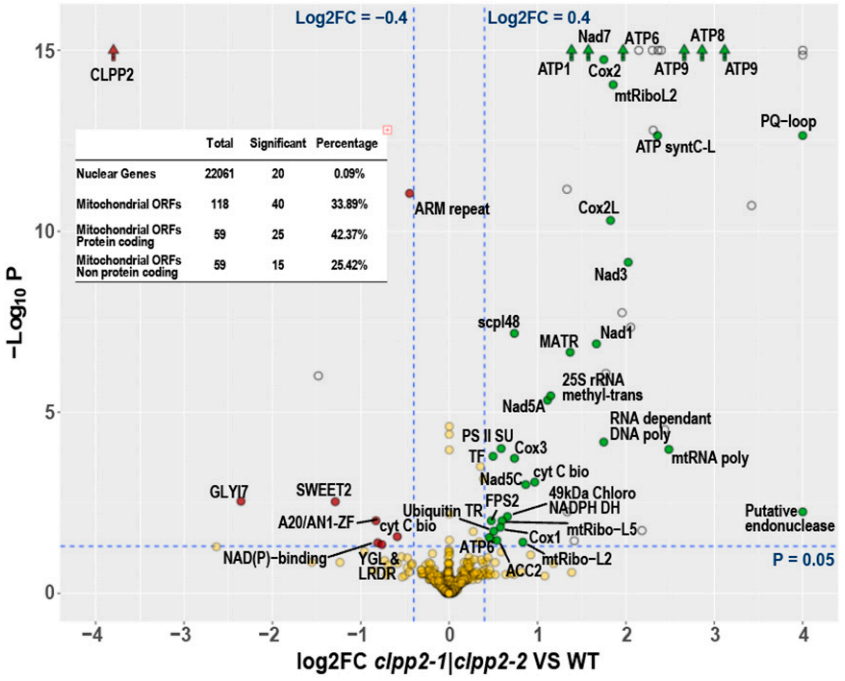

Figure 2. Changes in global transcript abundances in *CLPP2* mutants compared with the wild type (WT). The volcano plot illustrates overlapping significant changes of total transcript abundances of the two knockout mutants compared to the wild type. The negative Log10 transformed adjusted *P*-values are plotted against the log2FC of the transcript abundances measured by RNAseq. Dashed lines separate gene transcripts with significant changes in abundance using the log2FC cutoff of ±0.4 and adjusted *P*-value cutoff of 0.05. Depleted gene transcripts are shown in red and accumulated gene transcripts in green. Transcripts with adjusted *P*-values $<1 \times 10^{-15}$ are indicated by arrows. Transposable elements and hypothetical proteins are indicated by open circles. The inset table displays a summary of the total numbers of detected nuclear and mitochondrial genes and the numbers in each category with significant changes in abundance for both mutants relative to the wild type. ORF, Open reading frame.

target of human antibodies targeting cytoplasmic vesicle-like structures (Marchler-Bauer et al., 2017; El-Gebali et al., 2019).

Of the 41 upregulated mitochondrial-localized DEGs, 39 originate from the mitochondrial genome (Table 1) and encode proteins of the oxidative phosphorylation (OXPHOS) system, mitochondrial biogenesis apparatus, and various hypothetical proteins, transposons, and retrotransposons. Notably, the expression level of mitochondrial DEGs encoding complex V ATP synthase subunits (such as ATP1, ATP6 [ATMG00410, ATMG01170], ATP8, and ATP9) was higher in both CLPP2 mutants compared to the wild type (Table 1). Some mitochondrial genes encoding complex I subunits (NAD1, NAD3, NAD5, and NAD7) and complex IV subunits (COX1–COX3) were also observed to have high expression in both mutants (Table 1). Expression of mitochondrial genes encoding RNA or DNA polymerase (ATMG00490 and ATMG00810) and intron maturase (ATMG00520) were upregulated in both mutants (Table 1).

Loss of CLPP2 Alters Mitochondrial Protein Homeostasis

To identify differentially expressed proteins (DEPs) in isolated mitochondria from hydroponically grown Arabidopsis seedlings, we conducted a quantitative proteomic approach. We detected 797 proteins from mitochondrial membrane fractions in mutants and the wild type (see Supplemental Table S2). Among them, we identified 22 DEPs with increased abundance and five DEPs with decreased abundance. These showed a consistent pattern in *clpp2-1* and *clpp2-2*, with a log2FC exceeding ±0.4 and *P*-values ≤0.05 (Fig. 3). The 27 DEPs are are grouped based on functional categories in Table 2, with a description of each protein. We detected accumulation of ATP2 (AT5G08690) for complex V and four subunits of complex I (24 kD [AT4G02580], 51 kD [AT5G08530], 75 kD [AT5G37510], and B14 [AT3G12260]; Table 2). Three of the overaccumulated complex I subunits belong to the N-module of the matrix arm, which is assembled before it is attached to the membrane arm of complex I (Ligas et al., 2019). We observed accumulation of proteins related to protein synthesis, such as three components of the mito-ribosome (AT4G3090, AT1G61870, and AT5G64670) and the putative RNA helicase RH9 (AT3G22130), as well as mitochondrial proteases such as MPPα-1,α-2; MPPβ, CLPX-1, and PREP1 (Table 2). MPPs are mitochondrial peptidases that are embedded in complex III and are responsible for mitochondrial presequence cleavage after protein import (Braun et al., 1992; Zhang et al., 2001). CLPX-1 is the chaperone subunit of the CLPXP complex (van Wijk, 2015) and PREP1 degrades mitochondrial presequences after their cleavage from proteins (Kmiec and Glaser, 2012; Kmiec et al., 2014). A change to the abundance of these proteases in the absence of CLPP2 could influence the degradative landscape within the mitochondria of the *CLPP2* mutants. In addition to analysis of the membrane mitochondrial proteome, an analysis of matched samples of the soluble mitochondrial proteome produced similar results (including changes in the abundance of the 24-kD subunit, RH9, CLPX1, mtHSP70-1, and PPR proteins), albeit with different ratios of abundance for a range of proteins (including MPP, ATP2, and ATP3; Supplemental Fig. S2; Supplemental Table S2).

To investigate a potential modification in presequence processing or partial degradation of mature

Table 1. *Functional category of genes with significant changes in transcript abundance exceeding the cutoff in* clpp2-1 *and* clpp2-2

Genes were classified into the following groups: mitochondrial-encoded (mito-encoded), nuclear-encoded (nuc-encoded), plastid encoded, and knockout (nuclear encoded CLPP2 protease knocked out in the mutants; KO). The log2FC for both mutants compared to the wild type and the corresponding adjusted *P*-values (*P*.adj) are shown, as are gene symbols (with their complex) and Arabidopsis gene identifiers (AGI), short gene descriptions, and subcellular localization of the proteins based on the SUBA4 database. CI, Complex I; CIV, complex IV; CV, complex V; Cyt, cytosol; ER, endoplasmic reticulum; EX, extracellular; M, mitochondrion; N, nucleus; P, plastid; PM, plasma membrane; V, vacuole.

Group	Symbol	AGI	Description	Location	Log2FC *clpp2-1*	Log2FC *clpp2-2*	*P*.adj *clpp2-1*	*P*.adj *clpp2-2*
Mito-encoded	Nad3 (CI)	ATMG00990	NADH dehydrogenase 3	M	2.0	2.0	0.00	0.00
Mito-encoded	Nad1 (CI)	ATMG00516	NADH dehydrogenase 1C	M	1.7	1.7	0.00	0.00
Mito-encoded	Nad7 (CI)	ATMG00510	NADH dehydrogenase subunit 7	M	1.6	2.1	0.00	0.00
Mito-encoded	Nad5A (CI)	ATMG00513	NADH dehydrogenase 5A	M	1.1	1.5	0.00	0.00
Mito-encoded	Nad5C (CI)	ATMG00060	NADH dehydrogenase subunit 5C	M	0.9	1.3	0.00	0.00
Mito-encoded	Cox2L (CIV)	ATMG01280	Cytochrome C oxidase subunit II-like	M	1.8	2.3	0.00	0.00
Mito-encoded	Cox2 (CIV)	ATMG00160	Cytochrome oxidase 2	M	1.7	2.0	0.00	0.00
Mito-encoded	Cox3 (CIV)	ATMG00730	Cytochrome c oxidase subunit 3	M	0.7	1.2	0.00	0.00
Mito-encoded	Cox1 (CIV)	ATMG01360	Cytochrome oxidase	M	0.6	0.9	0.02	0.00
Mito-encoded	ATP9 (CV)	ATMG01090	ATP synthase 9	M	3.1	3.2	0.00	0.00
Mito-encoded	ATP8 (CV)	ATMG00480	Atp8	M	3.1	2.9	0.00	0.00
Mito-encoded	ATP9 (CV)	ATMG01080	F0-ATPase subunit 9	M	2.8	2.7	0.00	0.00
Mito-encoded	ATPsyntC-L (CV)	ATMG00040	ATP synthase subunit C family protein	M	2.4	3.0	0.00	0.00
Mito-encoded	ATP6 (CV)	ATMG00410	ATPase subunit 6-1	M	2.0	2.1	0.00	0.00
Mito-encoded	ATP1 (CV)	ATMG01190	ATP synthase subunit 1	M	1.4	1.8	0.00	0.00
Mito-encoded	ATP6 (CV)	ATMG01170	ATPase	M	0.5	0.9	0.03	0.00
Mito-encoded	mtRNA poly	ATMG00490	Mitovirus RNA polymerase	M	2.5	2.9	0.00	0.00
Mito-encoded	mtRibo L2	ATMG00980	Ribosomal protein S12/S23	M	1.9	1.9	0.00	0.00
Mito-encoded	DNA/RNA polymerase	ATMG00810	DNA/RNA polymerases	M	1.7	2.2	0.00	0.00
Mito-encoded	MATR	ATMG00520	Intron maturase	M	1.4	1.6	0.00	0.00
Mito-encoded	cyt C bio	ATMG00180	Cytochrome *C* biogenesis 452	M	1.0	1.4	0.00	0.00
Mito-encoded	mtRIbo L2	ATMG00560	Nucleic acid-binding	M	0.8	1.5	0.04	0.00
Mito-encoded	mtRibo L5	ATMG00210	Ribosomal protein L5	M	0.6	1.0	0.01	0.00
Mito-encoded	cyt C bio	ATMG00900	Cytochrome *C* biogenesis 256	M	−1.4	−0.6	0.00	0.03
Nuc-encoded	PQ-Motif	AT4G36850	PQ-loop repeat family protein	PM	16.0	16.9	0.00	0.00
Nuc-encoded	Putative endonuclease	AT3G56730	Endonuclease or glycosyl hydrolase	N,Cyt	6.7	8.1	0.01	0.00
Nuc-encoded	25S rRNA methyl-trans	AT4G26600	Methyltransferases	N	1.5	1.1	0.00	0.00
Nuc-encoded	scpl48	AT3G45010	Ser carboxypeptidase-like 48	EX	1.2	0.7	0.00	0.00
Nuc-encoded	ACC2	AT1G36180	Acetyl-CoA carboxylase 2	P	0.6	0.5	0.03	0.01
Nuc-encoded	Ubiquitin TR	AT5G63760	RING/U-box superfamily protein	N	0.5	1.0	0.02	0.00
Nuc-encoded	FPS2	AT4G17190	Farnesyl diphosphate synthase 2	M,Cyt	0.5	0.5	0.01	0.00
Nuc-encoded	TF	AT5G27410	D-Aminoacid aminotransferase-like	Cyt	0.5	0.6	0.00	0.00
Nuc-encoded	NAD(P)-binding	AT2G17845	NAD(P)-binding Rossmann-fold	M	−0.8	−2.0	0.04	0.00
Nuc-encoded	ARM repeat	AT3G56210	ARM repeat superfamily protein	M	−0.8	−0.4	0.00	0.00
Nuc-encoded	A20/AN1-ZF	AT1G12440	A20/AN1-like zinc finger protein	N	−1.1	−0.8	0.01	0.01
Nuc-encoded	SWEET2	AT3G14770	Nodulin MtN3 protein	V	−1.3	−1.3	0.00	0.00
Nuc-encoded	YGL&LRDR	AT3G15450	YGL and LRDR motifs	Per,Cyt	−1.9	−0.8	0.00	0.05
Nuc-encoded	GLYI7	AT1G80160	Lactoylglutathione lyase	Cyt,ER,PM	−2.4	−2.8	0.00	0.00
Plastid encoded	49 kD Chl NADPH DH	ATCG01110	49 kD SU Chloroplast NAD(P)H-DH	P	0.7	0.9	0.01	0.00
Plastid encoded	PSII SU	ATCG00280	PSII reaction center protein C	P	0.6	0.9	0.00	0.00
KO	CLPP2	AT5G23140	NCLPP2	M	−4.3	−4.7	0.00	0.00

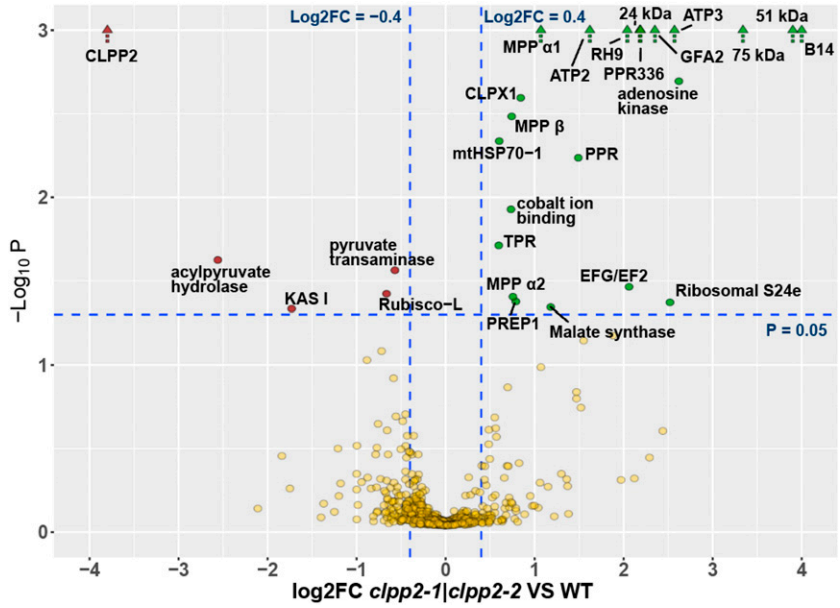

Figure 3. Changes in protein abundances in the membrane fraction of isolated mitochondria in *CLPP2* mutants compared with the wild type (WT). The volcano plot illustrates overlapping significant changes of label-free quantification protein intensities of the two knockout mutants compared to the wild type, using a log2FC cutoff of ±0.4 and an adjusted *P*-value cutoff of 0.05 (dashed blue lines). Depleted proteins are shown in red and accumulated proteins in green. Proteins with adjusted *P*-values $<1 \times 10^{-15}$ are displayed as arrows.

proteins, we conducted an approach combining protein labeling with isobaric tags for relative and absolute quantification (Ross et al., 2004) and charge-based fractional diagonal chromatography (ChaFRADIC; Venne et al., 2013, 2015) to analyze the N-terminal mature sequence of mitochondrial proteins. Sequence logo analysis indicated that there was no difference in presequence cleavage, as there were very conserved -2R and -3R cutting sites detected in mitochondrial proteins in both mutants and wild type (Supplemental Fig. S3, A and B**)**. There was also no apparent difference in the abundance of any presequence peptides between mutants and wild type (Supplemental Fig. S3C). In addition, no significant difference was observed in cleavage sites in the middle or C terminus of the protein sequence between the two mutants and the wild type (Supplemental Fig. S3, C and D). Thus, loss of CLPP2 had no measurable impact on mitochondrial protein maturation and left no partially degraded parts of mitochondrial proteins that we could detect.

Loss of CLPP2 Disrupts the Coordination of Mitochondrial- and Nuclear-Encoded Subunits of Respiratory and Ribosomal Complexes

To directly compare between mitochondrial transcript and protein abundance changes for individual subunits located in the same protein complex, we compiled the changes in transcript level and protein abundance for all subunits of the mitochondrial OXPHOS system and the mitochondrial ribosome (Fig. 4). Complex I, the largest protein complex of the mitochondrial OXPHOS system, is encoded by nine mitochondrial-encoded genes and 47 nuclear-encoded genes (Ligas et al., 2019; Meyer et al., 2019). Our data showed a consistent transcript upregulation for five mitochondrial-encoded subunits (NAD1, NAD3, NAD5, and NAD7) in both mutants, but we did not find NAD7 protein accumulation in either mutant (Fig. 4A). By contrast, complex I subunits (24 kD, 51 kD, 75 kD, and B14), encoded by four nuclear genes, showed high protein abundance with no change in transcript levels (Fig. 4A). A similar pattern was observed for complex V: of six mitochondrial transcripts, five (ATP1, ATP6 [ATMG0041 and ATMG01170], ATP7, and ATP8) had higher abundance in both mutants, but ATP1 and ATP8 did not show any accumulation at the protein level (Fig. 4E). There was no consistent transcript upregulation of nuclear genes encoding complex V subunits in either mutant, but there was high accumulation of the ATP2 protein, encoded by the nuclear genome, in both mutants (Fig. 4E).

Complex III contains only one mitochondrial-encoded subunit (Braun and Schmitz, 1992; Meyer et al., 2019), and its expression appeared to be unaffected transcriptionally in both mutants. Changes in protein abundance of MPPα-1, MPPα-2, and MPPβ were observed, but without any changes in transcript level for these nuclear-encoded genes (Fig. 4C). Complex IV has three mitochondrial subunits, with all showing up-regulation in transcript abundance in both mutants compared to the wild type, and 13 nuclear-encoded subunits of complex IV showed no change in transcript or protein abundance (Fig. 4D). Complex II of the OXPHOS system contains only nuclear-encoded subunits and appeared to not be affected by a disruption of the mitochondrial CLPP2 protease at the transcript or protein level (Fig. 4B). We did not find consistent transcriptional response in either CLPP2 mutant for mitochondrial-encoded subunits of the mito-ribosome (Fig. 4F); however, two nuclear-encoded ribosomal large subunits (AT4G30930 and AT5G64670)

Table 2. *Functional category of proteins with significant changes in abundance in clpp2-1 and clpp2-2*

Proteins were classified as OXPHOS, mitochondrial biogenesis (mtBIO), Protein homeostasis, knockout (nuclear encoded CLPP2 protease knocked out in the mutants; KO), and other (ungrouped genes). The log2FC of protein abundance in both mutants compared to the wild type, and the corresponding adjusted *P*-values (*P*.adj) are shown, as are the gene symbol, Arabidopsis gene identifier (AGI), a short description, and the subcellular protein localization based on the SUBA4 database.Cyt, Cytosol; ER, endoplasmic reticulum; EX, extracellular; M, Mitochondrion; N, nucleus; P, plastid; PM, plasma membrane; V, vacuole.

Group	Symbol	AGI	Description	Location	Log2FC *clpp2-1*	Log2FC *clpp2-2*	*P*.adj *clpp2-1*	*P*.adj *clpp2-2*
OXPHOS	B14	AT3G12260	B14 subunit of complex I	M	4.6	4.8	0.00	0.00
OXPHOS	51 kD	AT5G08530	51-kD subunit of complex I	M	4.4	4.7	0.00	0.00
OXPHOS	75 kD	AT5G37510	75-kD subunit of complex I	M	3.3	3.5	0.00	0.00
OXPHOS	ATP3	AT2G33040	γ subunit of mtATP synthase	M	2.6	2.8	0.00	0.00
OXPHOS	24 kD	AT4G02580	24-kD subunit of complex I	M	2.2	2.2	0.00	0.00
OXPHOS	ATP2	AT5G08690	ATP synthase α/β family protein	M	1.6	1.8	0.00	0.00
OXPHOS	MPPα-1	AT1G51980	Mitochondrial processing peptidase alpha 1	M	1.1	1.3	0.00	0.00
OXPHOS	MPPα-2	AT3G16480	Mitochondrial processing peptidase alpha 2	M	0.9	0.8	0.00	0.04
OXPHOS	MPPβ	AT3G02090	Mitochondrial processing peptidase beta	M	0.7	0.8	0.00	0.00
mtBio	Ribosomal S24e	AT5G02740	Ribosomal protein S24e family protein	M	2.5	2.8	0.00	0.04
mtBio	RH9	AT3G22310	Putative mitochondrial RNA helicase 1	M	2.5	2.0	0.00	0.00
mtBio	GFA2	AT5G48030	Gametophytic factor 2	M	2.4	2.4	0.00	0.00
mtBio	PPR336	AT1G61870	Pentatricopeptide repeat 336	M	2.2	2.2	0.00	0.00
mtBio	EFG/EF2	AT2G45030	Translation elongation factor EFG/EF2	M	2.1	2.4	0.00	0.03
mtBIO	PPR	AT1G10270	Gln-rich protein 23	M	1.5	1.5	0.00	0.01
Protein homeostasis	CLPX1	AT5G53350	CLP protease regulatory subunit X	M	0.9	0.8	0.00	0.00
Protein homeostasis	PREP1	AT3G19170	Presequence protease 1	M,P	0.8	0.8	0.00	0.04
Protein homeostasis	mtHSP70-1	AT4G37910	Mitochondrial heat shock protein 70-1	M	0.6	0.7	0.00	0.01
Other	adenosine kinase	AT2G37250	Adenosine kinase	P	2.6	2.6	0.00	0.00
Other	MLS	AT5G03860	Malate synthase	Per	1.2	2.9	0.05	0.00
Other	cobalt ion binding	AT3G15000	Cobalt ion binding	M	0.7	0.9	0.00	0.01
Other	TPR	AT1G26460	Tetratricopeptide repeat-like protein	M	0.6	0.7	0.00	0.02
Other	pyruvate transaminase	AT3G22200	Pyridoxal phosphate-dependent transferases	M	−0.6	−0.8	0.01	0.03
Other	Rubisco-L	ATCG00490	Ribulose-bisphosphate carboxylase large SU	P	−0.7	−0.9	0.01	0.04
Other	KAS I	AT5G46290	3-ketoacyl-acyl carrier protein synthase	P	−1.7	−2.3	0.01	0.05
Other	acylpyruvate hydrolase	AT4G15940	Fumarylacetoacetate hydrolase	M	−2.6	−2.9	0.00	0.02
KO	CLPP2	AT5G23140	CLPP2	M	−5.5	−5.4	0.00	0.00

and one nuclear-encoded ribosomal PPR336 (AT1G61870) increased in protein abundance in both mutants (Fig. 4F).

Loss of CLPP2 Impacts Protein Homeostasis and Incorporation of New Subunits into Complex I

Changes in the transcript level and protein abundance of specific complex I subunits led us to assess the impact on respiratory chain complex I in both mutants as an exemplar of a complex affected in *CLPP2* mutants. We first analyzed complex I activity in both mutants compared to the wild type as the rate of de-amino NADH-dependent FeCN reduction but did not find any difference in enzymatic activity (Fig. 5A). To determine the abundance of assembled complex I, we separated mitochondrial complexes using BN-PAGE and stained gels to visualize proteins with Coomassie (Fig. 5B). We did not observe any accumulation of complex I or supercomplex I+III_2 in either mutant compared with the wild type (Fig. 5B). Complex I in gel activity staining using NADH and nitroblue tetrazolium

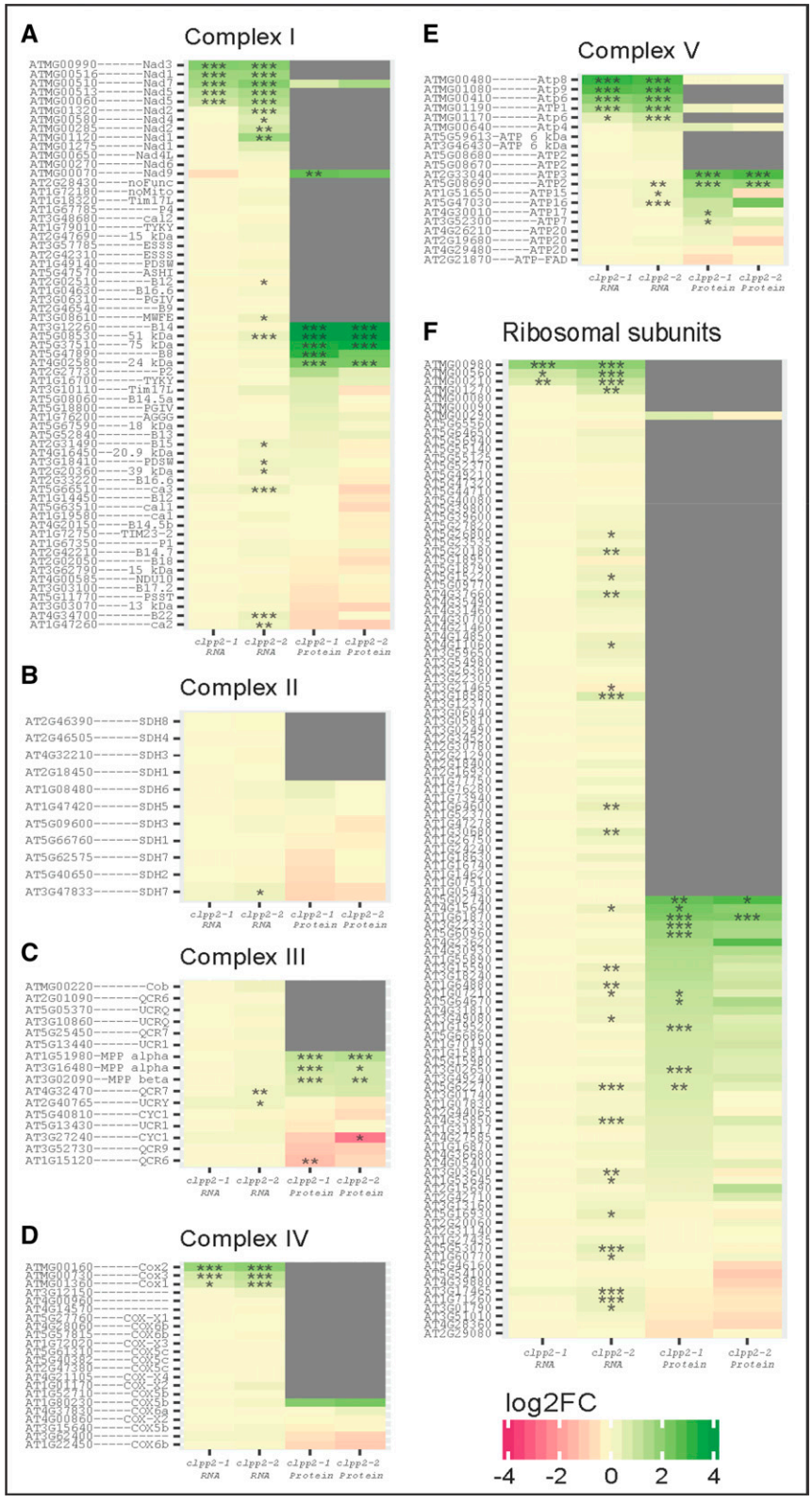

Figure 4. Changes in transcript and protein abundance from OXPHOS and ribosome complexes in *CLPP2* mutants. Shown are data for complexes I (A), II (B), III (C), IV (D), and V (E), and the mitochondrial ribosomal complex (F). The heatmaps show the combined changes in transcript abundance (from RNAseq data; Fig. 2) and protein abundance (from quantitative proteomics data; Fig. 3) for the RNA and proteins indicated. The subunits with accession number and abbreviations from individual complexes are listed at the left. In heatmaps, the color code represents the log2FC of the individual mutants compared to the wild type, with green for accumulation and red for depletion in the mutants. Gray indicates undetected proteins. Asterisks indicated significant difference (*$P \leq 0.05$, **$P \leq 0.01$, and ***$P \leq 0.001$; $n = 3$ for transcripts and 4 for proteins).

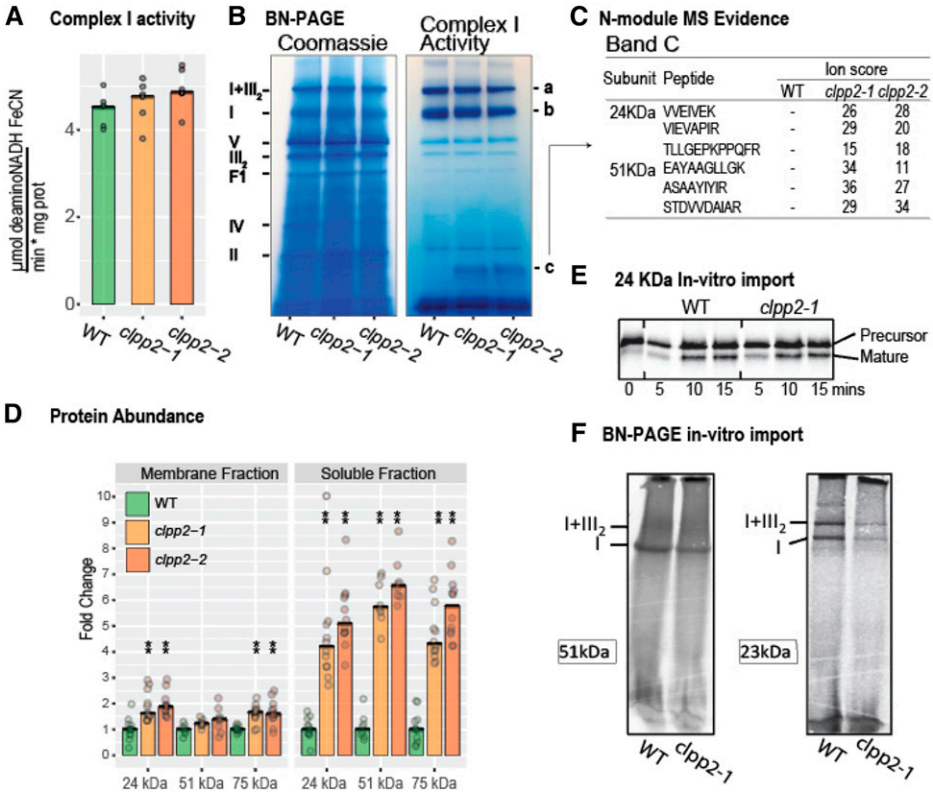

Figure 5. Changes in protein abundance for complex I N-module subunits and complex I enzymatic activity and in vitro import for complex I subunits in *CLPP2* mutants. A, Complex I enzyme activity in isolated mitochondria from mutants and the wild type (WT) using de-amino NADH as substrate and FeCN as donor. Measurements were made by photospectrometer assay ($n = 5$). B, BN-PAGE of isolated mitochondria of the wild type, *clpp2-1*, and *clpp2-2* stained with Coomassie blue (left) and complex I activity stain (NADH and NBT; right). Major OXPHOS components are marked on the gel for size comparison. Lowercase letters at right indicate bands of interest: supercomplex $I+III_2$ (a), complex I (b), and a potential complex I assembly intermediate (c). C, MS evidence for N-module proteins (24 and 51 kD) present in band c in the BN-PAGE. D, Protein abundance of three complex I matrix arm N-module subunits (24, 51, and 75 kD) in membrane and soluble fractions from isolated mitochondria. Data are shown as log2FC in peptide abundance compared to the wild-type median. Asterisks indicated significant difference (**$P \leq 0.01$; $n = 4$). E, In vitro import of the radio-labeled 24-kD subunit of complex I into isolated mitochondria of the wild type and *clpp2-1* at 5, 10, and 15 min incubation. F, In vitro import of radio-labeled complex I 51- and 23-kD subunits into isolated mitochondria of the wild type and *clpp2-1* at 2 h incubation time. The blue-native gels were imaged for radioactive intensity. Loading control gels stained with Coomassie blue are presented in Supplemental Figure S4.

(NBT) as substrate (Yan et al., 2007) showed that supercomplex $I+III_2$ (band a) and complex I (band b) had similar in-gel activity in both mutants and wild type (Fig. 5B), consistent with their protein abundance and total complex I enzymatic activity. However, we found a residual in-gel activity stain in a lower-molecular-mass complex (band c) in both mutants but not in the wild type (Fig. 5B). This indicated the existence of a potential subcomplex of complex I containing a functional FMN cofactor to convert NADH to NAD^+ and to transfer the free electron onto NBT. To further confirm this hypothesis, we cut the gel band c region from both mutants and wild type and subjected them to mass spectrometry (MS) analysis. We detected 51- and 24-kD subunits of complex I in both mutants but not in the wild type (Fig. 5C), pointing to the existence of a substantial amount of a soluble unassembled N-module subcomplex. We then measured the protein abundance of the three accumulated N-module subunits (24, 51, and 75 kD) by targeted MRM MS in purified mitochondria after fractionation into membrane and soluble fractions by centrifugation. In the membrane fraction, a significant 1.5- to 2-fold accumulation of the 24- and 75-kD subunits in *clpp2-1* and *clpp2-2* was observed when compared to the wild type (Fig. 5D). However, in the soluble fraction, accumulation was 4- to 6.5-fold that of the wild type and significant for all three subunits (Fig. 5D). This indicated that the accumulation of specific complex I N-module subunits appeared to be an accumulation of an unassembled subcomplex even though the steady-state intact complex I abundance was not affected in either mutant.

We conducted an in vitro protein import assay of a radio-labeled 24-kD subunit to understand the nature of the accumulation of the upregulated complex I subunits in *clpp2*. After cloning and expression, the ^{35}S Met-labeled

24-kD subunit was incubated with freshly isolated mitochondria. We did not observe any apparent difference in the rate of import between the wild type and *clpp2-1* (Fig. 5E). We then tested the incorporation of the radio-labeled 24-kD subunit into complex I using BN-PAGE analysis, but we failed to detect any obvious bands that would suggest incorporation within a protein complex. (Supplemental Fig. S4). Therefore, we tested another complex I N-module component, the 51-kD subunit (Fig. 5F). After 2 h of import, the radio-labeled, 51-kD subunit was observed to incorporate into complex I in the wild type and *clpp2-1*, with a stronger signal observed in the wild type (Fig. 5F). We then selected the 23-kD Q-module subunit that is known to interact with the N-module (Ligas et al., 2019). Weaker labeling of complex I and supercomplex $I+III_2$ with the 23-kD subunit was observed in *clpp2-1* compared with the wild type (Fig. 5F). To determine whether the labeling pattern was different with other complex I subunits, we selected the P-module CAL1 subunit and the membrane arm component, B14.7 subunit (Ligas et al., 2019; Supplemental Fig. S4). After 2 h of import of those subunits, we observed stronger labeling of complex I and supercomplex $I+III_2$ bands in the wild type compared to *clpp2-1* (Supplemental Fig. S4). We conclude that for all four subunits tested, labeled subunits can be incorporated into complex I and supercomplex $I+III_2$ and that this incorporation appeared weaker in mitochondria isolated from *clpp2-1* compared to wild-type mitochondria.

Plants Endure Loss of Mitochondrial CLPP2 under Normal and Stress Conditions

We evaluated the growth of *clpp2-1* and *clpp2-2* compared to wild-type plants under a range of growth conditions to find any phenotypical consequences caused by loss of mitochondrial CLPP2. Arabidopsis seedlings grown for 2 weeks under long-day control conditions showed no phenotypic differences between the wild type, *clpp2-1*, and *clpp2-2* (Fig. 6A). In mouse (*Mus musculus*) myoblasts, disruption of mitochondrial CLPP is known to lead to an altered mitochondrial morphology (Deepa et al., 2016). Plant roots are a mitochondria-rich tissue for energy production without chloroplasts. We employed transmission electron microscopy to investigate the morphology of CLPP2-deficient Arabidopsis mitochondria in root tissues and found no visible differences between the wild type, *clpp2-1*, and *clpp2-2* (Fig. 6B). We grew Arabidopsis seedlings on vertical Murashige and Skoog media agar plates to investigate root elongation under control and various stress conditions. Under control conditions (Fig. 6C) and various stress conditions (salt, osmotic stress, heat, and carbon starvation; Supplemental Fig. S5), we did not find significant changes in root elongation between the wild type and either *clpp2-1* or

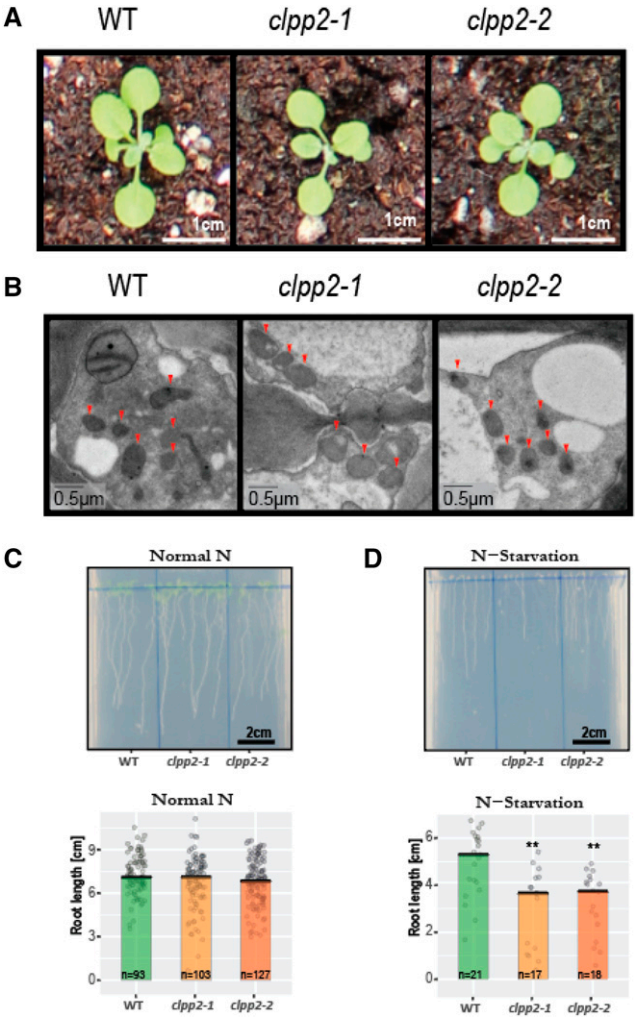

Figure 6. Phenotypes associated with loss of mitochondrial CLPP2 under different conditions. A, Arabidopsis seedlings of the wild type (WT), *clpp2-1*, and *clpp2-2* grown on soil for 15 d under long-day conditions. B, Representative transmission electron microscope images of dissected roots of 2-week-old hydroponically grown Arabidopsis seedlings of the wild type, *clpp2-1*, and *clpp2-2*. Mitochondria are indicated by red arrows. C and D, Representative plate images (top) and root-length measurements (bottom) of 2-week-old Arabidopsis seedlings grown on vertical plates under control long-day conditions under normal nitrogen supply (C) or without nitrogen (D). Dots represent individual root measurements. Asterisks indicated significant difference (**$P \leq 0.01$).

clpp2-2. We also treated plants with inhibitors of complex I (rotenone), complex III (antimycin A), and the mitochondrial biogenesis inhibitor (doxycycline), but again no difference in growth was found (Supplemental Fig. S5). So far, the only stress condition that affected *clpp2-1* and *clpp2-2* differently from the wild type was nitrogen starvation, which, after 14 d (Fig. 6D), showed significant reduction in root growth to ~60% of the wild-type root length. Therefore, Arabidopsis seedlings can compensate for the loss of CLPP2 under most growth conditions, but under nitrogen starvation scenarios it

appears that CLPXP may help to acclimate to stress conditions efficiently.

DISCUSSION

CLPP has been well studied in bacteria and some eukaryotes, such as human (*Homo sapiens*), mice, and fungi, and in particular in the plant chloroplast, where it plays an essential role in chloroplast biogenesis and development (Yu and Houry, 2007; van Wijk, 2015; Bhandari et al., 2018). While it has long been known that a CLPP exists in plant mitochondria (Peltier et al., 2004), there was no information on its function due to lack of genetic resources for its disruption and analysis. In this study, we successfully developed two mutant lines using CRISPR-Cas9 to knock out the Arabidopsis mitochondrial *CLPP2* gene. These mutants were designed to provide direct insight into CLPP2 function both in mitochondrial protein homeostasis and in coordinated regulation of assembly of plant respiratory complex subunits, which exhibit mixed mitochondrial and nuclear genomic location.

To our surprise, the knockout of mitochondrial *CLPP2* did not cause any phenotypic variation in either CRISPR-Cas9 mutant when compared with the wild type (Fig. 6). By contrast, the plastid-encoded CLPP1 in tobacco plays an essential role in shoot development (Shikanai et al., 2001). In Arabidopsis, CLPP4 and CLPP5 null mutants were embryo lethal, and null mutants of CLPP3 were seedling lethal in soil. Partial down-regulation of *CLPP4* and *CLPP6* by antisense RNA techniques reduced plant growth and development and resulted in pale green plants (Sjögren et al., 2006; Zheng et al., 2006; Olinares et al., 2011). Unlike its chloroplast counterpart, the plant mitochondrial CLPP appears to not be essential for plant growth and development. As bacteria lack a proteasome protein degradation system, CLPP and LON proteases contribute to ~80% of their cellular protein degradation (Goldberg et al., 1994). Bacterial CLPP plays an important role in the degradation of proteins involved in nutrient starvation, stationary phase adaptation, heat-stress response, cell-cycle progression, biofilm formation, cell motility, and metabolism (Frees et al., 2003; Gerth et al., 2008). The plant mitochondrial LON protease plays a key role in regulation of mitochondrial protein homeostasis, and loss of mitochondrial LON1 causes a severe reduction in plant growth and development (Rigas et al., 2009; Solheim et al., 2012; Li et al., 2017). By contrast, there is no information on the function of Lon protease in chloroplastic protein degradation, even though one isoform, LON4, is targeted to the chloroplast (Ostersetzer et al., 2007). The contrasting roles of CLPP and LON proteases in chloroplasts and plant mitochondria might indicate a shift from Lon protease to CLP protease for the respective regulation of critical aspects of chloroplastic and mitochondrial protein homeostasis.

Dysfunction of mitochondrial CLPP causes significant phenotypes in other eukaryotes. Loss of mitochondrial CLPP in humans is linked to infertility and sensorineural hearing loss (Gispert et al., 2013; Szczepanowska et al., 2016). Mitochondrial CLPP in humans is required for protein homeostasis (Szczepanowska et al., 2016), which is involved in the degradation and regulation of several enzymes of the electron transport chain and other cellular metabolic pathways such as mitochondrial translation/tRNA modification, mitochondrial transcription, protein folding, and proteolysis (Fischer et al., 2013; Cole et al., 2015; Szczepanowska et al., 2016). Loss of mitochondrial CLPP in mice leads to general infertility in both males and females, reduction in physical growth, and sensorineural deafness (Gispert et al., 2013; Szczepanowska et al., 2016). Remarkably, deletion of mitochondrial CLPP leads to improved health and increased life span in the filamentous fungus *Podospora anserina* (Fischer et al., 2013). In this study, loss of plant mitochondrial CLPP did not result in any apparent defects in plant growth and development. Therefore, mitochondrial CLPP has diverse impacts on growth and development based on phenotypic analysis among different eukaryotic organisms, potentially due to redundant roles in the mitochondrial protease network.

In this study, we observed that loss of CLPP2 affected the expression of only ~0.1% of nuclear genes (Fig. 2A) but nearly 33% of mitochondrial genes (Fig. 2A), indicating an important impact of this protease on the landscape of mitochondrial gene expression patterns. Mitochondrial ATP-dependent proteases, such as LON and CLPP, are proposed to serve roles in mitochondrial DNA functions including packaging and stability, replication, transcription, and translation (Matsushima and Kaguni, 2012). CLPP may play an indirect role in the regulation of mitochondrial DNA replication, transcription, and translation (Matsushima and Kaguni, 2012). We observed that loss of CLPP2 caused high expression levels of genes encoding potential RNA/DNA polymerases (ATM00490 and ATMG00810), a putative intron maturase (ATMG00520), and a nucleic acid-binding protein (ATMG00560; Fig. 2). In addition, the abundance of mitochondrial RNA helicases RH9 (AT3G22310; Fig. 3) and RH53 (AT3G22330; Supplemental Fig. S2) increased in both mutants relative to the wild type. Similarly, the protein abundance of chloroplast AtRH3 (AT5G26742), which is closely related to mitochondrial RH9 and RH53 (Asakura et al., 2012), was strongly (>5-fold) accumulated in *clpr2-1* and *clpr4-1* (Rudella et al., 2006; Kim et al., 2009; Zybailov et al., 2009). Chloroplast RH3 DEAD Box RNA Helicases in maize (*Zea mays*) and Arabidopsis function in splicing of specific group II introns and affect chloroplast ribosome biogenesis (Asakura et al., 2012). So far, there is no detailed information on the global impact of loss of chloroplast CLPP on expression of chloroplastic genes, but such studies are likely to be hard to interpret given the severity of the plastid phenotypes of these mutants.

The effect of CLPP2 loss on mitochondrial accumulation of nuclear-encoded proteins for complexes with mixed subunits derived from both mitochondrial and nuclear genomes can be easily seen for complex I, complex V, and the mito-ribosome (Fig. 4, A, E, and F).

This is reminiscent of previous evidence that a post-translational process is responsible for balancing the availability of nuclear subunits for complex assembly (Sarria et al., 1998; Giegé et al., 2005). We have shown through a detailed examination of complex I that this effect is primarily due to an excess of subunit availability and not to a block on import, preprotein processing, or accumulation of assembled and functional complexes, indicating that CLPP2 prevents such protein accumulations. It is known that CLPP targets subunits within protein complexes in a range of other organisms, providing a housekeeping mechanism for mixed-origin complexes (Flynn et al., 2003; Feng et al., 2013; Fischer et al., 2013; Szczepanowska et al., 2016). Indeed, Arabidopsis orthologs of CLPP substrates identified by trapping approaches in other organisms (including the 24- and 75-kD subunits of complex I) were identified as DEPs in this study (Supplemental Table S3).

Whereas Giegé et al. (2005) previously identified the phenomenon of nonstoichiometry of mixed-origin subunits in a transition from starved to refed Arabidopsis callus culture cells, we found here that carbon starvation did not produce a phenotype in *clpp2* plants (Supplemental Fig. S5), but transient response to nitrogen starvation did (Fig. 6). This implies that non-stoichiometric accumulation of unused subunits is not in itself egregious for plant mitochondrial function (Fig. 5; Supplemental Fig. S5). The reasons for the specific need for mixed subunit complexes to turn over in this way are unknown. However, there is additional evidence for such maintenance of complex I. The nuclear-encoded matrix arm subunits of complex I, including the 75-kD, 51-kD, 39-kD, 18-kD, and B17.2 subunits, exhibited relatively higher turnover rates compared to other subunits of complex I in Arabidopsis (Li et al., 2013). Blue native activity assays and targeted proteomic analysis indicated that the N-module subcomplex was highly accumulated in the matrix fraction in both mutants, indicating increased stability of this separated part of complex I in *clpp2* plants (Fig. 5; Supplemental Fig. S6). In CLPP-deficient mice, reduced protein levels in complex I subunits have also been observed (Deepa et al., 2016; Szczepanowska et al., 2016). Recently, it was discovered that turnover of the N-module within BN-PAGE-purified intact mitochondrial complexes was faster in proliferating than in differentiated mammalian cell cultures (Szczepanowska et al., 2020). It was proposed that ClpXP protease plays a key role in complex I maintenance, acting through surveillance and replacement of expended N-modules (Szczepanowska et al., 2020). It was shown that to regenerate stalled complex I, ClpXP can recognize, disassemble, and rapidly degrade impaired N-module proteins, allowing an effective replacement of N-module components in preexisting complex I (Szczepanowska et al., 2020). In plants, it is still not clear how dysfunction of CLPP2 impairs the incorporation of complex I subunits into complex I and supercomplex $I+III_2$ based on in vitro import analyses (Fig. 5F; Supplemental Fig. S4); however, this new work in mammalian systems provides a hypothesis to be tested. Future work on in vivo protein turnover using stable isotope progressive labeling (Li et al., 2017) would be required to dissect the impact of CLPP2 on the assembly versus the repair of protein complexes in plants.

MATERIALS AND METHODS

CRISPR-Cas9-Guided Mutagenesis of *clpp2*

The guide RNAs were designed for each target at *CLPP2* exon1 using CRISPRdirect (Naito et al., 2015) and were further analyzed with E-CRISPR (Heigwer et al., 2014). The cassettes containing two guide RNAs for each mutant were ordered as gBlocks and were inserted into the pHEE2E backbone, provided by Dr. Qi-Jun Chen (Wang et al., 2015), by restriction-ligation using BsaI (New England Biolabs; Supplemental Fig. S1). All plants were Arabidopsis (*Arabidopsis thaliana*) plants (ecotype Columbia-0) grown on soil as described below and were transformed by *Agrobacterium*-mediated DNA insertion using the floral-dipping procedure (Clough and Bent, 1998). Plants transformed with the CRISPR-Cas9 construct were selected by resistance to hygromycin (15 μg mL^{-1}). Genomic DNA was extracted from leaf tissue according to a protocol adapted from Edwards et al. (1991). Primers F1 (ATGAGGGGTCTCGTTTCC G) and R1 (GCCGCCAGGGGAATTGAGA) were used for PCR genotyping. Homozygous T1 plants were determined by the presence of a single trace including the desired mutations after Sanger sequencing. T2 plants were selected for the absence of CRISPR-Cas9 T-DNA by PCR. T2 and T3 seedlings were used for subsequent experiments.

Plant Growth

Arabidopsis seeds (wild type [Columbia-0] and CRISPR-Cas9 knockout mutants *clpp2-1* and *clpp2-2*) were sown on a perlite:vermiculite:compost (1:1:3; Seedling Substrate Plus+, Bord Na Móna) soil mix and covered with a transparent hood. After vernalization for 3 d at 4°C in the dark, plants were grown under control conditions: long-day photoperiod (16 h light at 150 μmol m^{-2} s^{-1} light intensity, 8-h-dark), 70% relative humidity, 22°C during the day and 18°C at night. For selection of transformed plants, seeds were spread on Murashige and Skoog Gamborg B5 plates (0.8% [w/v] agar, 1% [w/v] Suc, 0.05% [w/v] MES [pH 5.8 with KOH]), supplemented with 15 μg mL^{-1} hygromycin B, and placed in the dark at 4°C for 3 d. Then plates were transferred to long-day conditions as described above. For root length measurements, seeds were surface sterilized and placed on Murashige and Skoog Gamborg B5 plates as described above in a vertical orientation. For root stress treatments, Arabidopsis seedlings were grown on vertical Murashige and Skoog agar (pH 5.8, 1% [w/v] Suc) plates, with addition or removal of specific growth conditions: rotenone (addition of 5 μM rotenone), antimycin A (addition of 50 μM antimycin A), doxycycline (addition of 1 mg L^{-1} doxycycline), salt stress (addition of 100 mM NaCl), osmotic stress (addition of 175 mM mannitol), carbon starvation (no Suc supplied), and heat (seedlings on plates grown at 30°C day/night).

For mitochondria isolation and RNA extraction, Arabidopsis seeds were surface sterilized and dispensed into one-half strength Murashige and Skoog Gamborg B5 liquid media within enclosed, sterilized 100 mL polypropylene containers. The containers were seated on a rotating shaker in the long-day conditions as described above and seedlings were harvested 2 weeks after germination.

RNAseq Analysis

RNA was extracted from three biological replicates per genotype using the Spectrum Plant Total RNA Kit (Sigma-Aldrich) according to the instructions. The RNA quality and quantity were assessed using a nanodrop ND-1000 spectrophotometer (ThermoFisher). RNAseq library preparation and 50-bp single-end read sequencing on BGISEQ-500 was performed by the BGI Group. RNAseq data were received from BGI as fastq file format. Following quality control with FastQC (https://www.bioinformatics.babraham.ac.uk/projects/fastqc/), on average, 42 million reads were obtained per sample, and these were mapped to Arabidopsis reference genome Ensembl v34 and quantified with Salmon (v0.14.0; Patro et al., 2017). Differential analysis was

performed with the R package DESEQ2 (Love et al., 2014), and transcripts with a log2FC exceeding ±0.4 for the mutant relative to the wild type and an adjusted *P*-value ≤0.05 were considered differentially expressed.

RNA sequencing data was deposited to the Gene Expression Omnibus (Barrett et al., 2013) with the accession number GSE141942.

Mitochondria Isolation, Protein Purification, and Trypsin Digestion

The 2-week-old hydroponically grown Arabidopsis seedlings were used for mitochondria isolation (Lee et al., 2008). The isolated mitochondria were quantified using the Bradford (1976) method and the aliquots were stored at −80°C until further analysis.

For MRMs used to confirm CLPP2 loss at the protein level, 200 μg mitochondria was precipitated with 9× volumes ice-cold acetone for 24 h at −20°C and centrifuged at 20,000*g* for 20 min at 4°C. The pellets were collected for further analysis. For quantitative untargeted MS and MRM MS analysis of different mitochondrial fractions, 200 μg mitochondria were lysed using 3× freeze-thaw cycles (20 min at −20°C followed by 20 min at 4°C) and centrifuged at 20,000*g* for 20 min at 4°C. The supernatant (soluble fraction) and pellet (membrane fraction) were collected and precipitated with 9× volumes cold acetone for 24 h at −20°C. The pellets from soluble and membrane fractions were collected for further targeted MS analysis using MRM. For quantitative untargeted MS and MRM MS experiments, samples were alkylated and trypsin digested as follows:

The above acetone-precipitated pellets were resuspended with 100 μL solution containing 50 mM ammonium bicarbonate and 10 mM dithioreithol (pH 8.0), and incubated at 60°C for 30 min. Samples were cooled to room temperature and alkylated with 100 μL 50 mM ammonium bicarbonate and 25 mM iodoacetamide for 30 min. Samples were trypsin digested by adding digestion solution (1:50 [w/w] trypsin:protein), 50 mM ammonium bicarbonate, 2% (v/v) acetonitrile, 1.2 mM $CaCl_2$, and 0.1 M guanidine GuHCl [pH 8.0]) and incubated at 37°C for 16 h in a thermomix at 1,000 rpm. Digested samples were desalted and concentrated using C18 macroSpin columns (The Nest Group) according to the manufacturer's instructions and then eluted with 100 μL solution (80% [v/v] acetonitrile and 0.1% [v/v] formic acid). Elutes were dried under vacuum, resuspended in 2% (v/v) acetonitrile and 0.1% (v/v) formic acid to a final concentration of ~1 $\mu g\ \mu L^{-1}$ protein. Finally, samples were filtered through an Ultrafree-MC Centrifugal Filter (0.22 μm, polyvinylidene difluoride) according to the instructions of the manufacturer (MilliporeSigma).

Quantitative Untargeted MS

Samples with 1 μg protein were analyzed by liquid chromatography (LC)-MS on a Thermo orbitrap fusion mass spectrometer using data-dependent acquisition. Analysis consisted of direct injection onto a self-packed 150 mm × 75 μm Reprosil-Pur 120 C18-AQ 1.9-μm column (Dr. Maisch). Water/acetonitrile gradients with 0.1% (v/v) formic acid were formed by an Ultimate U3000 nano pump running at 250 nL min^{-1} from 2% to 27% (v/v) acetonitrile over 30 min.

Thermo raw files were database searched and quantified using MaxQuant (v1.6.7.0; Cox and Mann, 2008) and analyzed using the R package DEP (Zhang et al., 2018). Based on PCA analysis, one wild-type sample and one *clpp2-2* sample were flagged as outliers (showing high overall variance compared to all other samples) and removed.

Quantitative untargeted MS results have been deposited to the ProteomeXchange Consortium via the PRIDE (Perez-Riverol et al., 2019) partner repository with the dataset identifier PXD016746 (reviewer account details: Username, reviewer68924@ebi.ac.uk; Password, vRUlkOnv).

Targeted MRM MS

MRM MS was conducted as described previously (James et al., 2019). In brief, 10 μg protein in 10 μL of each sample were loaded onto an AdvanceBio Peptide Map column (2.1 × 250 mm, 2.7 μm particle size; part number 651750-902, Agilent), using an Agilent 1290 Infinity II LC System. The column was heated to 60°C. Peptides were eluted over a 15-min gradient (0–1 min, 3% [v/v] acetonitrile and 0.1% [v/v] formic acid to 8% [v/v] acetonitrile and 0.1% [v/v] formic acid; 1–15 min, 8% [v/v] acetonitrile and 0.1% [v/v] formic acid to 45% [v/v] acetonitrile and 0.1% [v/v] formic acid; 15–15.5 min, 45% [v/v] acetonitrile and 0.1% [v/v] formic acid to 100% [v/v] acetonitrile and 0.1% [v/v] formic acid; 15.5–16 min, 100% [v/v] acetonitrile and 0.1% [v/v] formic acid to 3% [v/v] acetonitrile and 0.1% [v/v] formic acid; 16–30 min, 3% [v/v] acetonitrile and 0.1% [v/v] formic acid) into the Agilent 6495 Triple Quadrupole MS for detection. Peptide transitions used for MRM are given in Supplemental Table S1.

Protein Labeling with Reagents for Isobaric Tags for Relative and Absolute Quantitation, ChaFRADIC, and LC-MS/MS Analysis of N-Terminal Peptides

In total, 12 samples corresponding to four biological replicates of each genotype i.e. wild type, *clpp2-1*, and *clpp2-1* were used and divided into two experiments. Briefly, isolated mitochondria pellets (~ 100 μg of protein) of each genotype and their respective biological replicates were first solubilized with 10 μL of 10% (w/v) SDS containing complete mini protease inhibitor cocktail and samples were diluted to 100 μL with 50 mM NH_4HCO_3 buffer (pH 7.8). Reduction and subsequent alkylation steps were carried out with 10 mM DTT and incubation at 56°C for 30 min; followed by alkylation of free thiol groups using 30 mM iodoacetamide and incubation at room temperature for 30 min in dark. Next, each sample was diluted 10-fold with ice-cold ethanol in 1:10 ratio, vortexed and stored at -40°C for 60 min followed by centrifugation in a pre-cooled (4°C) centrifuge at 18,000*g* for 30 min. Next, the supernatant was discarded and to each protein pellet 100 μL of ice-cold acetone were added, briefly vortexed, and centrifuged as above. The supernatant was discarded and the protein pellets were dried under a laminar flow hood. Labeling of proteins using reagents for isobaric tags for relative and absolute quantitation, enrichment of the N-terminal peptides based on the ChaFRADIC method, LC-MS/MS, and data analysis were performed as previously described (Venne et al., 2013, 2015).

MS proteomics data were deposited to the ProteomeXchange Consortium via the PRIDE (Perez-Riverol et al., 2019) partner repository with the dataset identifier PXD016263 (reviewer account details: Username, reviewer75079@ebi.ac.uk; Password, 2y7IvNFO).

Sequence Logo Analysis

Sequence logos of N-terminal peptides detected by ChaFRADIC MS were produced using the R package "ggseqlogo". Sequence logos are created from frequency data, whereas the ChaFRADIC MS results finally yield intensity data. The intensities were normalized and transformed into frequency data. RH9 (AT3g22310) and RH53 (AT3g22330) were identified as outliers (i.e. they contributed >50× sequences) and removed for this calculation. Transformation and normalization were performed using the following rules. The raw peptide intensity was normalized to the median of all peptide intensities. Transformation was achieved using a normalized intensity of ≤0.1 at a frequency of 1 followed by normalized intensity of ≤0.2 at a frequency of 2, and then increasing the frequency from 1 to 25 by 0.1 increments. Sequences were then multiplied based on their frequencies and the sequence logo was calculated.

Complex I Enzymatic Activity Assay

Complex I enzymatic assays were carried out as described previously (Huang et al., 2015). Deamino-NADH:Q reductase (complex I) specific activity was measured by the following reaction. The reaction solution contained 50 mM Tris-HCl [pH 7.2], 50 mM NaCl, 1 mM FeCN, and 0.2 mM deamino-NADH. The decrease in A_{420} at 25°C was recorded after adding 10 μg mitochondrial protein to a 1-mL reaction solution. The extinction coefficient of FeCN at 420 nm is 1.03 $mM^{-1}\ cm^{-1}$.

BN-PAGE and Complex I In-Gel Activity Staining

For gel separation, 300 μg mitochondrial proteins were dissolved with 5 mg digitonin mg $protein^{-1}$ and then separated with a 4.5% to 16% gradient BN-PAGE gel (Schertl and Braun, 2015). Part of the gel was stained with Coomassie blue. For the complex I in-gel activity assay, the gel was washed three times with distilled water for 5 min and incubated in the reaction medium (0.14 mM NADH, 1.22 mM NBT, and 0.1 M Tris-HCl [pH 7.4]). When the dark blue stain was strong enough, the reaction was stopped by transferring the gel to 40% (v/v) methanol and 10% (v/v) acetic acid (Schertl and Braun, 2015).

In-Gel Spot Identification

Gel spots (~1 mm^3) of interest were excised from the blue-native gel, destained twice in appropriate volumes of 50% (v/v) methanol:50% (v/v) 50 mM ammonium bicarbonate and 0.1% (v/v) formic acid for 30 min at 1,000 rpm, twice dehydrated in appropriate volumes of 50% (v/v) acetonitrile:50% (v/v) 50 mM ammonium bicarbonate and 0.1% (v/v) formic acid for 1 min, and for 30 s in 100% (v/v) acetonitrile. Samples were then reduced, alkylated, dehydrated, digested, and cleaned up as described above in appropriate volumes and identified using an Agilent 6550 Q-TOF as described previously (Nelson et al., 2014).

Protein Import Assays

[^{35}S]-Met-labeled proteins were translated using the rabbit reticulocyte TNT in vitro transcription translation kit (Promega) with the full-length complementary DNA of the 24-kD subunit (AT4G02580) cloned into pDEST14 as previously described (Ivanova et al., 2019). In vitro protein import assays were carried out as described previously in 30 μg of freshly isolated mitochondria (Duncan et al., 2015). BN-PAGE import assays were carried out using [^{35}S]-Met-labeled proteins as previously described (Duncan et al., 2015). In brief, radiolabeled protein was incubated with 30 μg of freshly isolated mitochondria for 2 h, and the mitochondria were pelleted by centrifugation and processed for BN-PAGE analysis (Eubel et al., 2005), except that commercially available precast native-PAGE gels were used (Novex Tris-Gly, Thermofisher). Full-length complementary DNAs of the 51-kD (AT5G08530) and 23-kD (AT1G79010) subunits, CAL1 (At5g63510), and B14.7 (At2g42210) of complex I were cloned using Gateway technology into pDONR201 and subsequently recombined into pDEST14 for [^{35}S]-Met-labeled protein translation as described above.

Transmission Electron Microscopy

Root tissues of 2-week-old hydroponic seedlings were used, and the analyses were performed in Australian National University's Electron Microscope laboratory according to the method described previously (Hyman and Jarvis, 2011). The dissected root tissues were fixed overnight in 2.5% (v/v) glutaraldehyde:2% (v/v) paraformaldehyde in 0.1 M sodium phosphate buffer (pH 7.2) and then postfixed with 1% (w/v) OsO4:1.5% (w/v) potassium ferricyanide. The tissues were then dehydrated gradually in ethanol and propylene oxide, embedded in Spurr's resin, and cured for 24 h at 70°C. Ultrathin sections~70 nm thick were cut using a Leica UC7 ultramicrotome, collected onto copper mesh grids, and stained with 1% (w/v) uranyl acetate and Reynolds' lead citrate. The images were taken with a Hitachi7100 transmission electron microscope at 75 kV. Images were acquired using a Gatan Orius CCD camera.

Accession Numbers

Sequence data from this article can be found in the GenBank/EMBL data libraries under accession numbers AT5G23140, AT5Gg53350, AT5G49840, and AT1G33360.

Supplemental Data

The following supplemental materials are available.

Supplemental Figure S1. Cloning history of the plasmid used to create the CRISPR-Cas9-mediated stable *CLPP2* knockout lines.

Supplemental Figure S2. Changes in protein abundances in the soluble fraction of isolated mitochondria from *CLPP2* mutants compared with the wild type.

Supplemental Figure S3. Sequence logos of N-terminal peptides obtained from ChaFRADIC MS of purified mitochondrial proteins from the wild type, *clpp2-1*, and *clpp2-2*.

Supplemental Figure S4. BN-PAGE separations of in vitro imports of radio-labeled complex I subunits to determine the rate of label incorporation into complex I and supercomplex $I+III_2$.

Supplemental Figure S5. Arabidopsis seedlings of the wild type, *clpp2-1*, and *clpp2-2* grown on Murashige and Skoog agar plates under stress conditions or additional chemicals.

Supplemental Figure S6. Schematic position of N-module subunits in complex I and the unassembled N-module subcomplex in the mitochondrial matrix.

Supplemental Table S1. Peptide transition list used for MRM MS analysis.

Supplemental Table S2. Changes in protein abundance in membrane and soluble fractions of isolated mitochondria in *CLPP2* mutants compared with the wild type.

Supplemental Table S3. List of subunits in mitochondrial complexes as substrates for CLPP targets through trapping approaches in other organisms.

Received February 6, 2020; accepted June 12, 2020; published June 22, 2020.

LITERATURE CITED

Asakura Y, Galarneau E, Watkins KP, Barkan A, van Wijk KJ (2012) Chloroplast RH3 DEAD box RNA helicases in maize and Arabidopsis function in splicing of specific group II introns and affect chloroplast ribosome biogenesis. Plant Physiol **159:** 961–974

Barrett T, Wilhite SE, Ledoux P, Evangelista C, Kim IF, Tomashevsky M, Marshall KA, Phillippy KH, Sherman PM, Holko M, et al (2013) NCBI GEO: Archive for functional genomics data sets—update. Nucleic Acids Res **41:** D991–D995

Bhandari V, Wong KS, Zhou JL, Mabanglo MF, Batey RA, Houry WA (2018) The role of ClpP protease in bacterial pathogenesis and human diseases. ACS Chem Biol **13:** 1413–1425

Bradford MM (1976) A rapid and sensitive method for the quantitation of microgram quantities of protein utilizing the principle of protein-dye binding. Anal Biochem **72:** 248–254

Braun H-P, Schmitz UK (1992) Affinity purification of cytochrome *c* reductase from potato mitochondria. Eur J Biochem **208:** 761–767

Braun HP, Emmermann M, Kruft V, Schmitz UK (1992) The general mitochondrial processing peptidase from potato is an integral part of cytochrome *c* reductase of the respiratory chain. EMBO J **11:** 3219–3227

Clough SJ, Bent AF (1998) Floral dip: A simplified method for *Agrobacterium*-mediated transformation of *Arabidopsis thaliana*. Plant J **16:** 735–743

Cole A, Wang Z, Coyaud E, Voisin V, Gronda M, Jitkova Y, Mattson R, Hurren R, Babovic S, Maclean N, et al (2015) Inhibition of the mitochondrial protease ClpP as a therapeutic strategy for human acute myeloid leukemia. Cancer Cell **27:** 864–876

Costanzo MC, Fox TD (1990) Control of mitochondrial gene expression in *Saccharomyces cerevisiae*. Annu Rev Genet **24:** 91–113

Couvillion MT, Soto IC, Shipkovenska G, Churchman LS (2016) Synchronized mitochondrial and cytosolic translation programs. Nature **533:** 499–503

Cox J, Mann M (2008) MaxQuant enables high peptide identification rates, individualized p.p.b.-range mass accuracies and proteome-wide protein quantification. Nat Biotechnol **26:** 1367–1372

Deepa SS, Bhaskaran S, Ranjit R, Qaisar R, Nair BC, Liu Y, Walsh ME, Fok WC, Van Remmen H (2016) Down-regulation of the mitochondrial matrix peptidase ClpP in muscle cells causes mitochondrial dysfunction and decreases cell proliferation. Free Radic Biol Med **91:** 281–292

Dong H, Fei G-L, Wu C-Y, Wu F-Q, Sun Y-Y, Chen M-J, Ren Y-L, Zhou K-N, Cheng Z-J, Wang J-L, et al (2013) A rice virescent-yellow leaf mutant reveals new insights into the role and assembly of plastid caseinolytic protease in higher plants. Plant Physiol **162:** 1867–1880

Duncan O, Carrie C, Wang Y, Murcha MW (2015) In vitro and in vivo protein uptake studies in plant mitochondria. In J Whelan, and MW Murcha, eds, Plant Mitochondria: Methods and Protocols Methods in Molecular Biology 1305. Springer New York, New York, pp 61–81

Edwards K, Johnstone C, Thompson C (1991) A simple and rapid method for the preparation of plant genomic DNA for PCR analysis. Nucleic Acids Res **19:** 1349

El-Gebali S, Mistry J, Bateman A, Eddy SR, Luciani A, Potter SC, Qureshi M, Richardson LJ, Salazar GA, Smart A, et al (2019) The Pfam protein families database in 2019. Nucleic Acids Res **47**(D1): D427–D432

Eubel H, Braun H-P, Millar AH (2005) Blue-native PAGE in plants: a tool in analysis of protein-protein interactions. Plant Methods **1:** 11

Feng J, Michalik S, Varming AN, Andersen JH, Albrecht D, Jelsbak L, Krieger S, Ohlsen K, Hecker M, Gerth U, et al (2013) Trapping and proteomic identification of cellular substrates of the ClpP protease in *Staphylococcus aureus*. J Proteome Res **12:** 547–558

Fischer F, Weil A, Hamann A, Osiewacz HD (2013) Human CLPP reverts the longevity phenotype of a fungal ClpP deletion strain. Nat Commun **4:** 1397

Flynn JM, Neher SB, Kim Y-I, Sauer RT, Baker TA (2003) Proteomic discovery of cellular substrates of the ClpXP protease reveals five classes of ClpX-recognition signals. Mol Cell **11:** 671–683

Frees D, Qazi SNA, Hill PJ, Ingmer H (2003) Alternative roles of ClpX and ClpP in *Staphylococcus aureus* stress tolerance and virulence. Mol Microbiol **48:** 1565–1578

Gerth U, Kock H, Kusters I, Michalik S, Switzer RL, Hecker M (2008) Clp-dependent proteolysis down-regulates central metabolic pathways in glucose-starved *Bacillus subtilis*. J Bacteriol **190:** 321–331

Giegé P, Hoffmann M, Binder S, Brennicke A (2000) RNA degradation buffers asymmetries of transcription in *Arabidopsis* mitochondria. EMBO Rep **1:** 164–170

Giegé P, Sweetlove LJ, Cognat V, Leaver CJ (2005) Coordination of nuclear and mitochondrial genome expression during mitochondrial biogenesis in *Arabidopsis*. Plant Cell **17:** 1497–1512

Gispert S, Parganlija D, Klinkenberg M, Dröse S, Wittig I, Mittelbronn M, Grzmil P, Koob S, Hamann A, Walter M, et al (2013) Loss of mitochondrial peptidase Clpp leads to infertility, hearing loss plus growth retardation via accumulation of CLPX, mtDNA and inflammatory factors. Hum Mol Genet **22:** 4871–4887

Goldberg AL, Moerschell RP, Chung CH, Maurizi MR (1994) ATP-dependent protease La (Lon) from *Escherichia coli*. In AJ Barrett, ed, Proteolytic Enzymes: Serine and Cysteine Peptidases, Methods in Enzymology 244. Elsevier, Amsterdam, pp 350–375

Heigwer F, Kerr G, Boutros M (2014) E-CRISP: Fast CRISPR target site identification. Nat Methods **11:** 122–123

Huang S, Lee CP, Millar AH (2015) Activity assay for plant mitochondrial enzymes. In J Whalen, and MW Murcha, eds, Plant Mitochondria: Methods and Protocols, Methods in Molecular Biology 1305. Springer, New York, pp 139–149

Huang S, Van Aken O, Schwarzländer M, Belt K, Millar AH (2016) The roles of mitochondrial reactive oxygen species in cellular signaling and stress response in plants. Plant Physiol **171:** 1551–1559

Hyman S, Jarvis RP (2011) Studying Arabidopsis chloroplast structural organisation using transmission electron microscopy. In RP Jarvis, ed, Chloroplast Research in Arabidopsis: Methods and Protocols, Vol I, Methods in Mmolecular Biology 774. Humana Press, Totowa, NJ, pp 113–132

Ivanova A, Gill-Hille M, Huang S, Branca R, Kmiec B, Teixeira PF, Lehtiö J, Whelan J, Murcha MW (2019) A mitochondrial LYR protein is required for Complex I assembly. Plant Physiol **181:** 1632–1650

James AM, Haywood J, Leroux J, Ignasiak K, Elliott AG, Schmidberger JW, Fisher MF, Nonis SG, Fenske R, Bond CS, et al (2019) The macrocyclizing protease butelase 1 remains autocatalytic and reveals the structural basis for ligase activity. Plant J **98:** 988–999

Kim J, Rudella A, Ramirez Rodriguez V, Zybailov B, Olinares PDB, van Wijk KJ (2009) Subunits of the plastid ClpPR protease complex have differential contributions to embryogenesis, plastid biogenesis, and plant development in *Arabidopsis*. Plant Cell **21:** 1669–1692

Kim J, Olinares PD, Oh SH, Ghisaura S, Poliakov A, Ponnala L, van Wijk KJ (2013) Modified Clp protease complex in the ClpP3 null mutant and consequences for chloroplast development and function in Arabidopsis. Plant Physiol **162:** 157–179

Kmiec B, Glaser E (2012) A novel mitochondrial and chloroplast peptidasome, PreP. Physiol Plant **145:** 180–186

Kmiec B, Teixeira PF, Glaser E (2014) Phenotypical consequences of expressing the dually targeted Presequence Protease, AtPreP, exclusively in mitochondria. Biochimie **100:** 167–170

Kühn K, Richter U, Meyer EH, Delannoy E, de Longevialle AF, O'Toole N, Börner T, Millar AH, Small ID, Whelan J (2009) Phage-type RNA polymerase RPOTmp performs gene-specific transcription in mitochondria of *Arabidopsis thaliana*. Plant Cell **21:** 2762–2779

Lee CP, Eubel H, O'Toole N, Millar AH (2008) Heterogeneity of the mitochondrial proteome for photosynthetic and non-photosynthetic *Arabidopsis* metabolism. Mol Cell Proteomics **7:** 1297–1316

Li L, Nelson C, Fenske R, Trösch J, Pružinská A, Millar AH, Huang S (2017) Changes in specific protein degradation rates in *Arabidopsis thaliana* reveal multiple roles of Lon1 in mitochondrial protein homeostasis. Plant J **89:** 458–471

Li L, Nelson CJ, Carrie C, Gawryluk RM, Solheim C, Gray MW, Whelan J, Millar AH (2013) Subcomplexes of ancestral respiratory complex I subunits rapidly turn over *in vivo* as productive assembly intermediates in *Arabidopsis*. J Biol Chem **288:** 5707–5717

Ligas J, Pineau E, Bock R, Huynen MA, Meyer EH (2019) The assembly pathway of complex I in *Arabidopsis thaliana*. Plant J **97:** 447–459

Lloyd JPB (2018) The evolution and diversity of the nonsense-mediated mRNA decay pathway. F1000 Res **7:** 1299

Love MI, Huber W, Anders S (2014) Moderated estimation of fold change and dispersion for RNA-seq data with DESeq2. Genome Biol **15:** 550

Marchler-Bauer A, Bo Y, Han L, He J, Lanczycki CJ, Lu S, Chitsaz F, Derbyshire MK, Geer RC, Gonzales NR, et al (2017) CDD/SPARCLE: Functional classification of proteins via subfamily domain architectures. Nucleic Acids Res **45**(D1): D200–D203

Matsushima Y, Kaguni LS (2012) Matrix proteases in mitochondrial DNA function. Biochim Biophys Acta **1819:** 1080–1087

McVey M, Lee SE (2008) MMEJ repair of double-strand breaks (director's cut): Deleted sequences and alternative endings. Trends Genet **24:** 529–538

Meyer EH, Welchen E, Carrie C (2019) Assembly of the complexes of the oxidative phosphorylation system in land plant mitochondria. Annu Rev Plant Biol **70:** 23–50

Millar AH, Whelan J, Soole KL, Day DA (2011) Organization and regulation of mitochondrial respiration in plants. Annu Rev Plant Biol **62:** 79–104

Moreno JC, Martínez-Jaime S, Schwartzmann J, Karcher D, Tillich M, Graf A, Bock R (2018) Temporal proteomics of inducible RNAi lines of Clp protease subunits identifies putative protease substrates. Plant Physiol **176:** 1485–1508

Moreno JC, Tiller N, Diez M, Karcher D, Tillich M, Schöttler MA, Bock R (2017) Generation and characterization of a collection of knock-down lines for the chloroplast Clp protease complex in tobacco. J Exp Bot **68:** 2199–2218

Naito Y, Hino K, Bono H, Ui-Tei K (2015) CRISPRdirect: Software for designing CRISPR/Cas guide RNA with reduced off-target sites. Bioinformatics **31:** 1120–1123

Nelson CJ, Alexova R, Jacoby RP, Millar AH (2014) Proteins with high turnover rate in barley leaves estimated by proteome analysis combined with in planta isotope labeling. Plant Physiol **166:** 91–108

Olinares PDB, Kim J, van Wijk KJ (2011) The Clp protease system; a central component of the chloroplast protease network. Biochim Biophys Acta **1807:** 999–1011

Ostersetzer O, Kato Y, Adam Z, Sakamoto W (2007) Multiple intracellular locations of Lon protease in Arabidopsis: Evidence for the localization of AtLon4 to chloroplasts. Plant Cell Physiol **48:** 881–885

Patro R, Duggal G, Love MI, Irizarry RA, Kingsford C (2017) Salmon provides fast and bias-aware quantification of transcript expression. Nat Methods **14:** 417–419

Peltier J-B, Ripoll DR, Friso G, Rudella A, Cai Y, Ytterberg J, Giacomelli L, Pillardy J, van Wijk KJ (2004) Clp protease complexes from photosynthetic and non-photosynthetic plastids and mitochondria of plants, their predicted three-dimensional structures, and functional implications. J Biol Chem **279:** 4768–4781

Perez-Riverol Y, Csordas A, Bai J, Bernal-Llinares M, Hewapathirana S, Kundu DJ, Inuganti A, Griss J, Mayer G, Eisenacher M, et al (2019) The PRIDE database and related tools and resources in 2019: Improving support for quantification data. Nucleic Acids Res **47**(D1): D442–D450

Rigas S, Daras G, Laxa M, Marathias N, Fasseas C, Sweetlove LJ, Hatzopoulos P (2009) Role of Lon1 protease in post-germinative growth and maintenance of mitochondrial function in *Arabidopsis thaliana*. New Phytol **181:** 588–600

Ross PL, Huang YN, Marchese JN, Williamson B, Parker K, Hattan S, Khainovski N, Pillai S, Dey S, Daniels S, et al (2004) Multiplexed protein quantitation in *Saccharomyces cerevisiae* using amine-reactive isobaric tagging reagents. Mol Cell Proteomics **3:** 1154–1169

Rudella A, Friso G, Alonso JM, Ecker JR, van Wijk KJ (2006) Down-regulation of ClpR2 leads to reduced accumulation of the ClpPRS protease complex and defects in chloroplast biogenesis in *Arabidopsis*. Plant Cell **18:** 1704–1721

Sarria R, Lyznik A, Vallejos CE, Mackenzie SA (1998) A cytoplasmic male sterility-associated mitochondrial peptide in common bean is post-translationally regulated. Plant Cell **10:** 1217–1228

Schelin J, Lindmark F, Clarke AK (2002) The clpP multigene family for the ATP-dependent Clp protease in the cyanobacterium *Synechococcus*. Microbiology **148:** 2255–2265

Schertl P, Braun H-P (2015) Activity measurements of mitochondrial enzymes in native gels. In J Whelan, and MW Murcha, eds, Plant Mitochondria: Methods and Protocols, Methods in Molecular Biology 1305. Springer, New York, pp 131–138

Senkler J, Senkler M, Eubel H, Hildebrandt T, Lengwenus C, Schertl P, Schwarzländer M, Wagner S, Wittig I, Braun H-P (2017) The mitochondrial complexome of *Arabidopsis thaliana*. Plant J **89:** 1079–1092

Shikanai T, Shimizu K, Ueda K, Nishimura Y, Kuroiwa T, Hashimoto T (2001) The chloroplast clpP gene, encoding a proteolytic subunit of ATP-dependent protease, is indispensable for chloroplast development in tobacco. Plant Cell Physiol **42:** 264–273

Sjögren LLE, Stanne TM, Zheng B, Sutinen S, Clarke AK (2006) Structural and functional insights into the chloroplast ATP-dependent Clp protease in *Arabidopsis*. Plant Cell **18:** 2635–2649

Smakowska E, Skibior-Blaszczyk R, Czarna M, Kolodziejczak M, Kwasniak-Owczarek M, Parys K, Funk C, Janska H (2016) Lack of FTSH4 protease affects protein carbonylation, mitochondrial morphology, and phospholipid content in mitochondria of Arabidopsis: New insights into a complex interplay. Plant Physiol **171:** 2516–2535

Solheim C, Li L, Hatzopoulos P, Millar AH (2012) Loss of Lon1 in Arabidopsis changes the mitochondrial proteome leading to altered metabolite profiles and growth retardation without an accumulation of oxidative damage. Plant Physiol **160:** 1187–1203

Szczepanowska K, Maiti P, Kukat A, Hofsetz E, Nolte H, Senft K, Becker C, Ruzzenente B, Hornig-Do H-T, Wibom R, et al (2016) CLPP coordinates mitoribosomal assembly through the regulation of ERAL1 levels. EMBO J **35:** 2566–2583

Szczepanowska K, Senft K, Heidler J, Herholz M, Kukat A, Höhne MN, Hofsetz E, Becker C, Kaspar S, Giese H, et al (2020) A salvage pathway maintains highly functional respiratory complex I. Nat Commun **11:** 1643

van Wijk KJ (2015) Protein maturation and proteolysis in plant plastids, mitochondria, and peroxisomes. Annu Rev Plant Biol **66:** 75–111

Venne AS, Solari FA, Faden F, Paretti T, Dissmeyer N, Zahedi RP (2015) An improved workflow for quantitative N-terminal charge-based fractional diagonal chromatography (ChaFRADIC) to study proteolytic events in *Arabidopsis thaliana*. Proteomics **15:** 2458–2469

Venne AS, Vögtle FN, Meisinger C, Sickmann A, Zahedi RP (2013) Novel highly sensitive, specific, and straightforward strategy for comprehensive N-terminal proteomics reveals unknown substrates of the mitochondrial peptidase Icp55. J Proteome Res **12:** 3823–3830

Wang Z-P, Xing H-L, Dong L, Zhang H-Y, Han C-Y, Wang X-C, Chen Q-J (2015) Egg cell-specific promoter-controlled CRISPR/Cas9 efficiently generates homozygous mutants for multiple target genes in *Arabidopsis* in a single generation. Genome Biol **16:** 144

Yan L-J, Yang S-H, Shu H, Prokai L, Forster MJ (2007) Histochemical staining and quantification of dihydrolipoamide dehydrogenase diaphorase activity using blue native PAGE. Electrophoresis **28:** 1036–1045

Yu AYH, Houry WA (2007) ClpP: A distinctive family of cylindrical energy-dependent serine proteases. FEBS Lett **581:** 3749–3757

Zhang X, Smits AH, van Tilburg GBA, Ovaa H, Huber W, Vermeulen M (2018) Proteome-wide identification of ubiquitin interactions using UbIA-MS. Nat Protoc **13:** 530–550

Zhang X-P, Sjöling S, Tanudji M, Somogyi L, Andreu D, Eriksson LEG, Gräslund A, Whelan J, Glaser E (2001) Mutagenesis and computer modelling approach to study determinants for recognition of signal peptides by the mitochondrial processing peptidase. Plant J **27:** 427–438

Zheng B, MacDonald TM, Sutinen S, Hurry V, Clarke AK (2006) A nuclear-encoded ClpP subunit of the chloroplast ATP-dependent Clp protease is essential for early development in *Arabidopsis thaliana*. Planta **224:** 1103–1115

Zybailov B, Friso G, Kim J, Rudella A, Rodríguez VR, Asakura Y, Sun Q, van Wijk KJ (2009) Large scale comparative proteomics of a chloroplast Clp protease mutant reveals folding stress, altered protein homeostasis, and feedback regulation of metabolism. Mol Cell Proteomics **8:** 1789–1810